CR 73082

SRS-TR150
19 March 1967

INVESTIGATION OF THE USE OF A RADIOISOTOPE FOR SPACE ENVIRONMENT SIMULATION

FINAL REPORT

SUBMITTED TO
NATIONAL AERONAUTICS AND SPACE ADMINISTRATION
AMES RESEARCH CENTER
MOFFET FIELD, CALIFORNIA
CONTRACT NAS2-3506

PHILCO-FORD CORPORATION
Space & Re-entry Systems Division
Palo Alto, California

SRS Technical Report 150
19 March 1967

INVESTIGATION OF THE USE OF A RADIOISOTOPE FOR SPACE ENVIRONMENT SIMULATION

Final Report

Submitted to

National Aeronautics and Space Administration
Ames Research Center
Moffett Field, California

Under Contract NAS2-3506

Submitted by: D M Newell
D. M. Newell
Project Engineer

Approved by: R F Lutz
R. F. Lutz, Manager
Materials Department

Approved by: R E Gaumer
R. E. Gaumer, Manager
Space Technology

Prepared by

PHILCO-FORD CORPORATION
Space and Re-entry Systems Division
Palo Alto, California

PHILCO
PHILCO-FORD CORPORATION

Space & Re-entry
Systems Division

TABLE OF CONTENTS

FIGURES

TABLES

ACKNOWLEDGEMENTS

The following personnel made contributions to the development of the Radiation Simulator (funded by Philco-Ford Corporation) and to the evaluation as a space environment simulator (funded by Ames Research Center).

D. M. Newell	Technical Leader
R. F. Lutz	Radioisotope source holder design and adaptation.
Dr. M. C. Rinehart	Electron spectral measurements.
M. A. Picciano	Optical reflectance measurements.
W. T. Picciano	Depth-dose computerization (Appendix A) Theoretical flux distribution (Appendix B)
W. E. Price	Thermoluminescent dosimetry.
D. B. Orvis	Ultraviolet, thermal control, and vacuum technology consulting.
C. J. Strombom	System maintenance and data collection.

SECTION 1

INTRODUCTION

The evaluation of many materials for application in space environments requires consideration of vacuum, solar electromagnetic radiation, corpuscular radiation, and the thermal environment. Reasonable means of simulation of these parameters have been achieved in man-made simulation chambers on earth with the exception of corpuscular radiation. This has most commonly been simulated in either monoenergetic or narrow energy band spectral increments, which have not been representative of the multienergetic spectra known to exist at various orbits.

Several investigators (References 1 through 5) have established that combined environments must be utilized for evaluation of materials such as external thermal control materials, solar cell assemblies, and certain electronic components. Such combined environmental tests are necessary because effects are dependent upon the type and energy spectrum of incident radiation, the rate of radiation energy deposition, the environment temperature, and environment atmosphere (gaseous) composition. Consecutive separate exposure of samples to the various environmental influences is not equivalent to combined environments testing since some of the mechanisms of change are inter-related; e.g., thermal annealing and radiation damage. Consequently, it was chosen in this program to utilize a beta-emitting radioisotope form amenable to incorporation in an environmental simulation chamber which already included control of the parametric variables of vacuum (gaseous environment), sample temperature, and solar electromagnetic radiation.

The primary aim of the program conducted by Philco-Ford, SRS Division, under contract NAS2-3506 was to demonstrate the feasibility of using a radioisotope to simulate the space electron environment. This report includes the theoretical and analytical bases for selection and design

of a sealed strontium 90-yttrium 90-titanate source, spectral calibration of the resultant source, electron dosimetry determinations at the sample sites within the chamber, operating experience, prototype specimen exposure test results, system evaluation, and conclusions and recommendations.

Report No. 1, WDL-TR-3002, covering Phase I of the contract and part of Phase II, was issued July, 1966.

Report No. 2, WDL-TR-3064, was a brief quarterly progress report.

SECTION 2

ANALYTICAL STUDIES

2.1 CHARACTERIZATION OF STRONTIUM-90 AS AN ELECTRON SOURCE

2.1.1 Spectra

Beta spectra for Sr^{90} and Y^{90} have been calculated by a theoretical approach(6) and are presented in Figures 2-1 and 2-2. To obtain the spectrum for an SR^{90}-Y^{90} source, the two spectra were combined under secular equilibrium conditions, resulting in the spectrum shown in Figure 3-4. The composite spectrum closely approximates a spectrum observed by E. Lamb, of Oak Ridge National Laboratory, on a video-tube screen(7), and also a previous theoretical spectrum published by the Atomic Energy Commission(8). Figures 2-1 and 2-2 are differential spectra. The ordinate is F(E)dE, and the area under the entire curve is equal to one. The area within any energy increment represents the fraction of the total number of electrons with that specified energy.

The spectra of other beta-emitting isotopes, i.e., P^{32}, Ru^{106}, As^{76}, K^{42}, Ce^{144}, and Cs^{137} were compared and found to be poor simulators for all orbits. In addition, all of the above mentioned isotopes have shorter half-lives; thus, having two distinct disadvantages when compared with Sr^{90}-Y^{90}.

One of the most important criteria for simulation is the absence of gammas from the decay process. All but one of the above-mentioned isotopes give off high-energy gammas in the decay process. Table 2-1 lists all seventeen of the radioisotopes considered for the simulator.

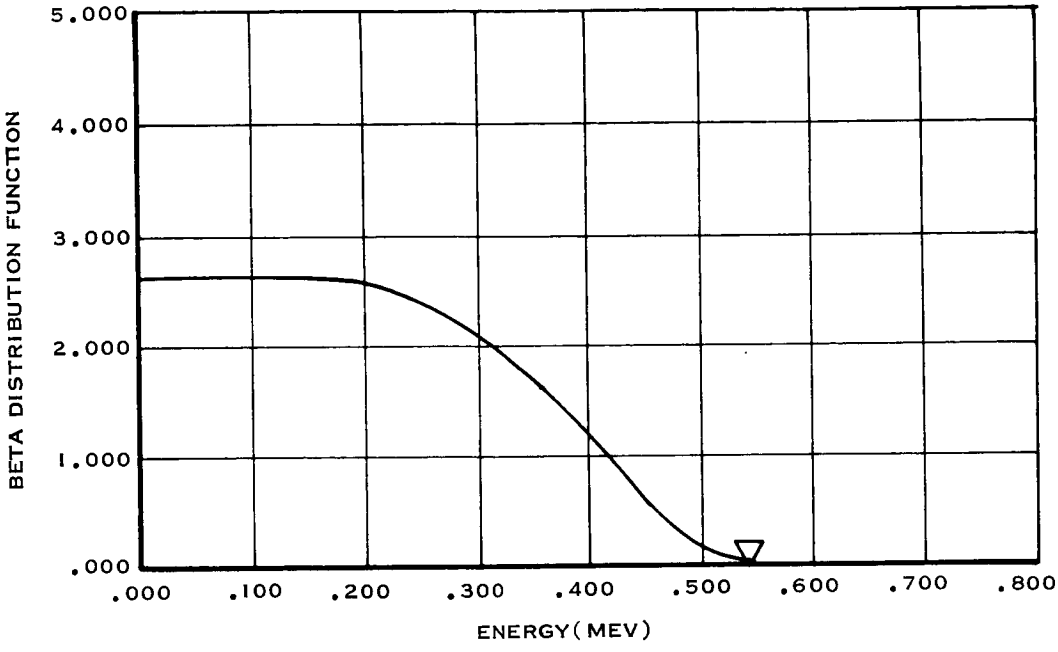

Figure 2-1 Strontium-90 Beta Spectrum

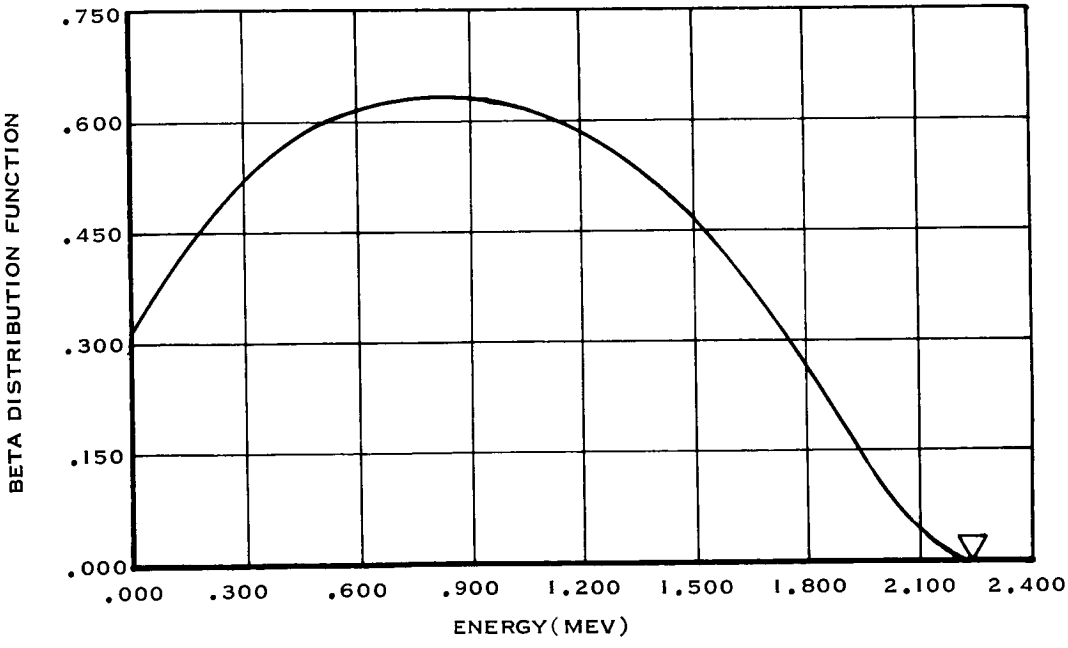

Figure 2-2 Yttrium-90 Beta Spectrum

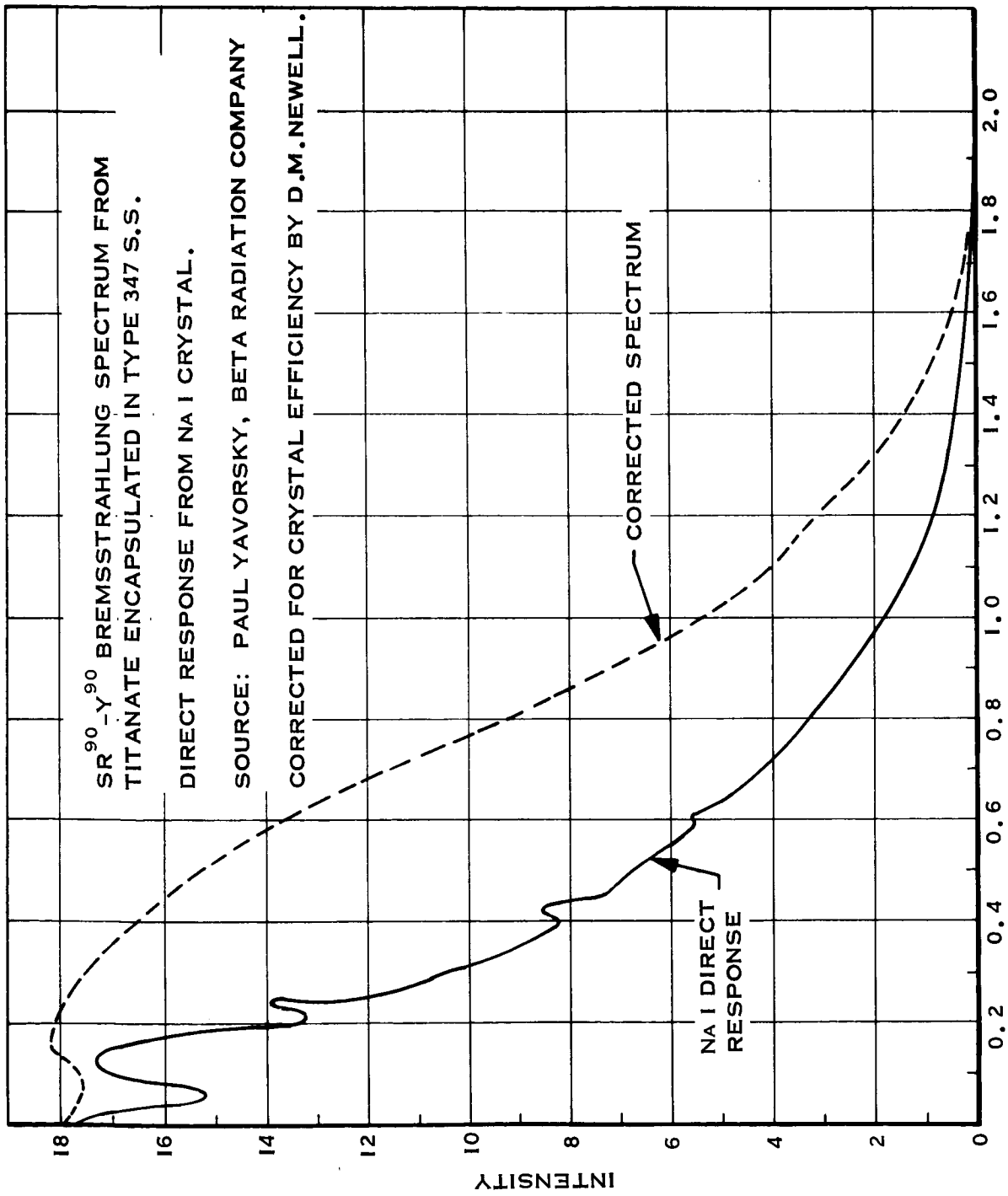

Figure 2-3 Sr^{90} - Y^{90} Bremsstrahlung Spectrum From Titanate Encapsulated in Type 347 S.S.

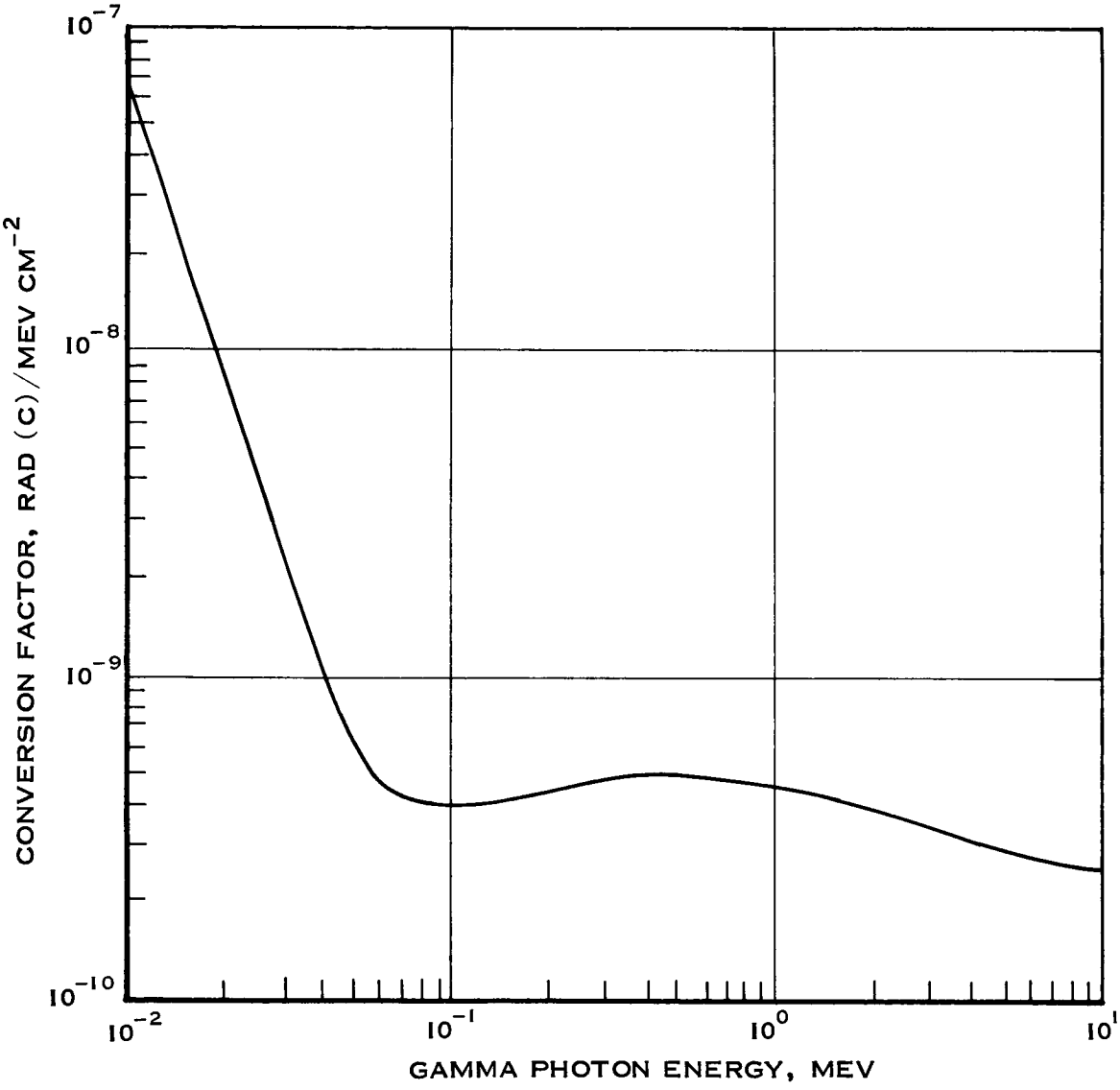

Figure 2-4 Gamma Energy-to-Dose Conversion Ratio

TABLE 2-1

EXAMPLES OF POTENTIAL ISOTOPES FOR SPACE SIMULATION CHAMBERS

Isotope	Half Life $t_{\frac{1}{2}}$	Maximum Energy (MEV)		Product	Product Stability
		β	γ		
Sr^{90}	28 yr.	0.57	None	Y^{90}	Unstable
Y^{90}	65 hr.	2.2	None**	Zr^{90}	Stable
P^{32}	14 day	1.7	None	S^{32}	Stable
Pm^{143}	14 day	0.9	None	Nd^{143}	Stable
Pm^{147}	2.7 yr.	0.23	None	Sm^{147}	Stable
Li^{8}*	0.88 Sec.	12	None	Be^{8}	Unstable (2α)
Be^{10}*	10^{6} yr.	0.56	None	B^{10}	Stable
B^{12}*	0.027 Sec.	13.4	4.4	C^{12}	Stable
Ru^{106}	1 yr.	0.04	None	Rh^{106}	Unstable
Rh^{106}	2.2 hr.	1.62	0.51, 0.22, 1.22	Pd^{106}	Stable
Rh^{106}	30 sec.	3.53	0.51, 0.62, 0.7, 3.4	Pd^{106}	Stable
As^{76}	26.5 hr.	2.97	0.56, 1.21	Se^{76}	Stable
K^{42}	12.4 hr.	3.53	1.52	Ca^{42}	Stable
Ce^{144}	285 day	0.32	0.134	Pr^{144}	Unstable
Pr^{144}	17.5 min.	3.15	2.18, 7.0	Nd^{144}	Stable
Cs^{137}	30 yr.	1.17	None	Ba^{137}	IT
Ba^{137}	2.6 min.	None	0.66	B^{137}	Stable

*The efficiency of reactor production or methods for in situ production of these isotopes have not been investigated.

** A 1.74 Mev gamma from Y^{90}, as previously reported, is now regarded as erroneous.

2.1.2 Isotopic Equilibrium

The combined Sr^{90}- Y^{90} spectrum referred to earlier can be achieved only at secular equilibrium of the two isotopes. Such an equilibrium occurs only in cases where the parent isotope has a very long half-life (Sr^{90} = 28 years) and the daughter isotope a relatively short half-life (Y^{90} = 64 hours).

In order to assure secular equilibrium of the purchased isotopic mixture, the minimum time to equilibrium was calculated. At any time (t), the following condition exists[9]:

$$\lambda_2 N_2 \approx \lambda_1 N_1^o \, (1-e^{-\lambda_2 t})$$

where:

λ_1 and λ_2 = disintegration constants for the two isotopes

N_2 = number of atoms of Y^{90} at time "t"

N_1^o = original number of Sr^{90} atoms

Now, at equilibrium, $\lambda_2 N_2 = \lambda_1 N_1$, and since $N_1 \approx N_1^o$ due to the long half-life of Sr^{90}, then equilibrium is reached when $(1-e^{-\lambda_2 t})$ approaches 1. This occurs when $e^{-\lambda_2 t}$ approaches 0. Evaluating for a low value ($e^{-\lambda_2 t} = 0.01$), one finds that secular equilibrium is reached at 430 hours, or about seven half-lives of Y^{90}. Since the isotopic source material was well over three weeks old when received, secular equilibrium was assured.

2.1.3 Physical Characteristics and Containment

Strontium titanate is a refractory ceramic, and the physical characteristics are determined by the properties of the individual oxides: SrO and TiO_2.

The physical properties (Table 2-2) are typical of high-temperature refractory oxides.

TABLE 2-2

PHYSICAL PROPERTIES OF SrO AND TiO_2

Property	SrO	TiO_2	$2Ti_2O_3.3TiO_2$
Spec. Gr.	4.7	3.84-4.26	----
Melting Pt., ^oC	2430	1825-1850	1640
Boiling Pt., ^oC	3000	2500-3000	----
Sol. in H_2O, g/100 cc	0.69	Insolvable	----
Heat of Vaporization (K cal./mole)	--	63-77	----

TiO_2 can decompose into $2Ti_2O_3.3TiO_2$, with a reaction equilibrium dependent upon the oxygen pressure and temperature. Since the evolved gas is nonradioactive, there is no more hazard involved in this potential oxygen evaluation than there would be from the desorption of absorbed gases from any surface.

It is nevertheless important that a leaky source does not release radioactivity into the vacuum system and exhaust. Radioactivity would have to contain Sr^{90}, and this cannot occur, even in the vicinity of a 1000-watt ultraviolet source, as the vapor pressures are too low.

2.1.4 Availability, Handling, and Shielding of Strontium-90 Sources

Oak Ridge National Laboratory is the basic domestic scource for Sr^{90}. It is supplied mostly as the titanate powder, but also as oxide, carbonate, and in ionic form. The highest concentrations of Sr^{90} are available only in the titanate and oxide forms. Oak Ridge will supply some standard forms of encapsulation, but does not attempt to compete with private industry in specialized packaging.

One of the best features of the present Philco-Ford source is the high concentration of Sr^{90}. The compacted strontium titanate has an activity of 32.54 curies/g and a density of 4.02 g/cc.

The total activity of the present Philco-Ford source is 5.96 curies of of Sr^{90}. Since it is in secular equilibrium with its shorter half-life daughter, Y^{90} there is, in essence, an additional 5.96 curies of Y^{90} available to the user.

The handling of a strontium source depends somewhat on the curie level and on the reliability of the encapsulation. During the design phase of the radiation source acquisition, a study of the bremsstrahlung radiation was made. It was determined that a cask assembly utilizing a minimum of 0.50 inch of lead in combination with 0.25 inch of steel was enough shielding for nonremote handling techniques. The following assumptions were made in the course of the calculations:

a. The steel-scattered spectrum, corrected for NaI efficiency, is correct (See Figure 2-3).

b. The conversion of Diethorn (10) of 0.0075 Mev gamma/electron disintegration is valid.

c. The four source rods are considered to be a point source for simplicity of shielding calculations.

The highest calculated dose rate outside the source holder was 2.1 inches from the center point, and is separated by 0.5 inch of lead and 0.25 inch of steel. For convenience, the steel was converted to an equivalent amount of lead in the calculations. The spectrum was divided into nine energy ranges in order to calculate μx, the gamma attenuation, at different energies. The transmitted flux, ϕ_T, was calculated in accordance with the equation $\phi_T = \phi_o e^{-\mu x}$. Flux values were then converted to roentgen with the help of Figure 2-4.

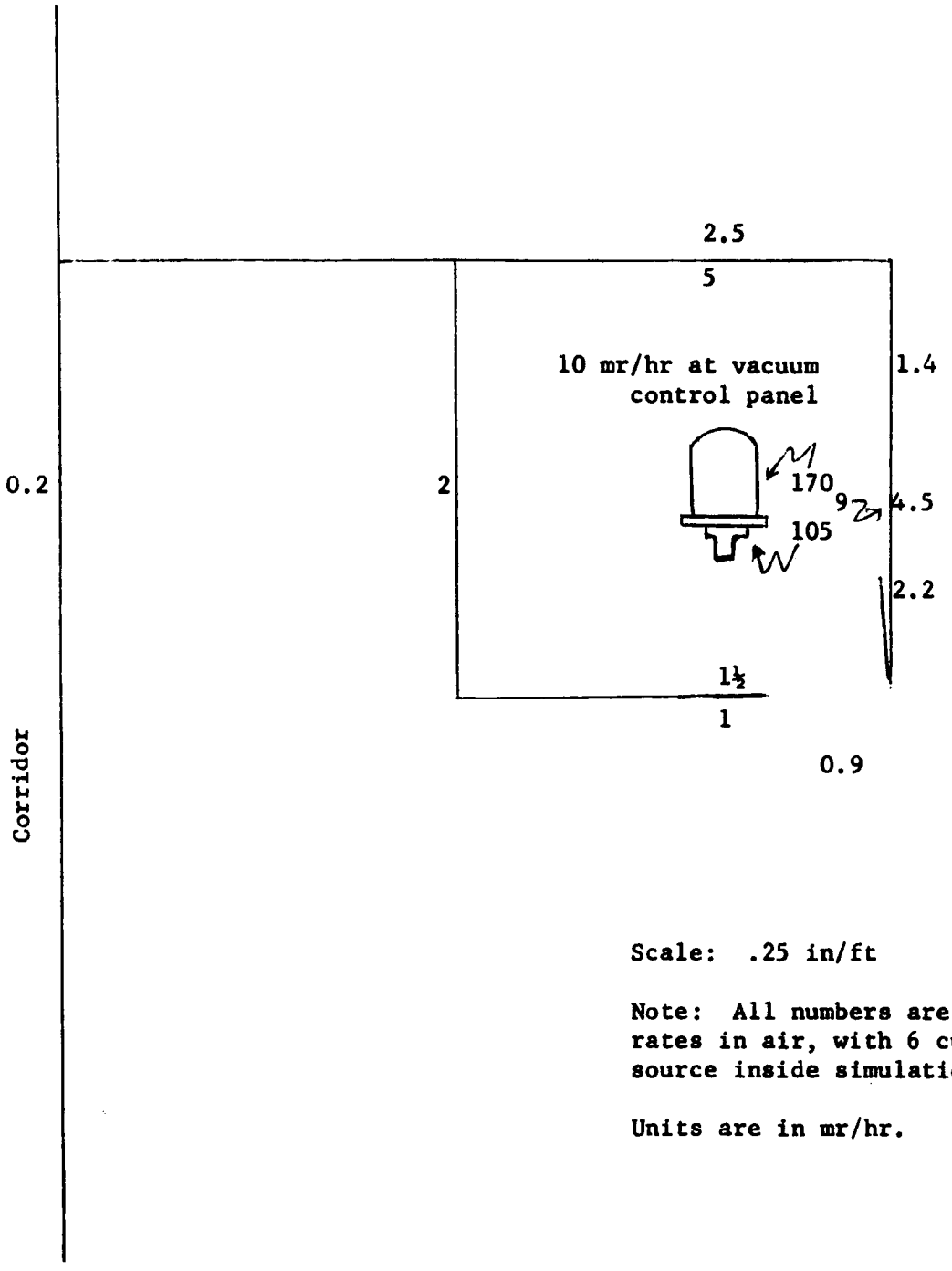

Figure 2-5. Radiation Dose Rate in and Around Controlled Area with Sr^{90} Source in Chamber

The true gamma dose rate when measured at this point, 170 mr/hr, was much lower, than the calculated value. Areas outside the source holder and outside the vacuum chamber have been mapped for gamma dose rates. The results of this mapping are illustrated in Figure 2-5.

2.1.5 Theoretical Flux Distribution

Since the radiation source consists of four 1-inch rods spatially distributed as shown in Figure 4-1, a simple point source calculation could not suffice for flux distribution. A detailed theoretical calculation was made based on the exact source rod geometry. This calculation is presented as Appendix B.

The calculation indicated that the dose rate at a distance of 5 inches from a sample looking at three source rods should be 28 percent higher than one looking at two source rods.

2.2 DEPTH-DOSE CALCULATIONS

When a sample is irradiated with electrons, it is known that the absorbed electron energy is not deposited linearly over the penetration range of the flux. There is a peak absorption about 1/3 of the range into the sample for every incident energy measured.

A functional relationship has been derived to fit experimental depth vs. dose data, and the resulting equations were arranged for convenient computer programming. The result is an explicit equation expressing the energy loss (or deposition) in each designated layer of a plane sample normally irradiated with a given spectrum of electron energies. The calculation is based on the assumption that the peak absorption at 1/3 of the electron range is valid.

The computer program, to perform this calculation, was developed and checked against hand calculated values (Fig. 2-6). After confirmation, the computer

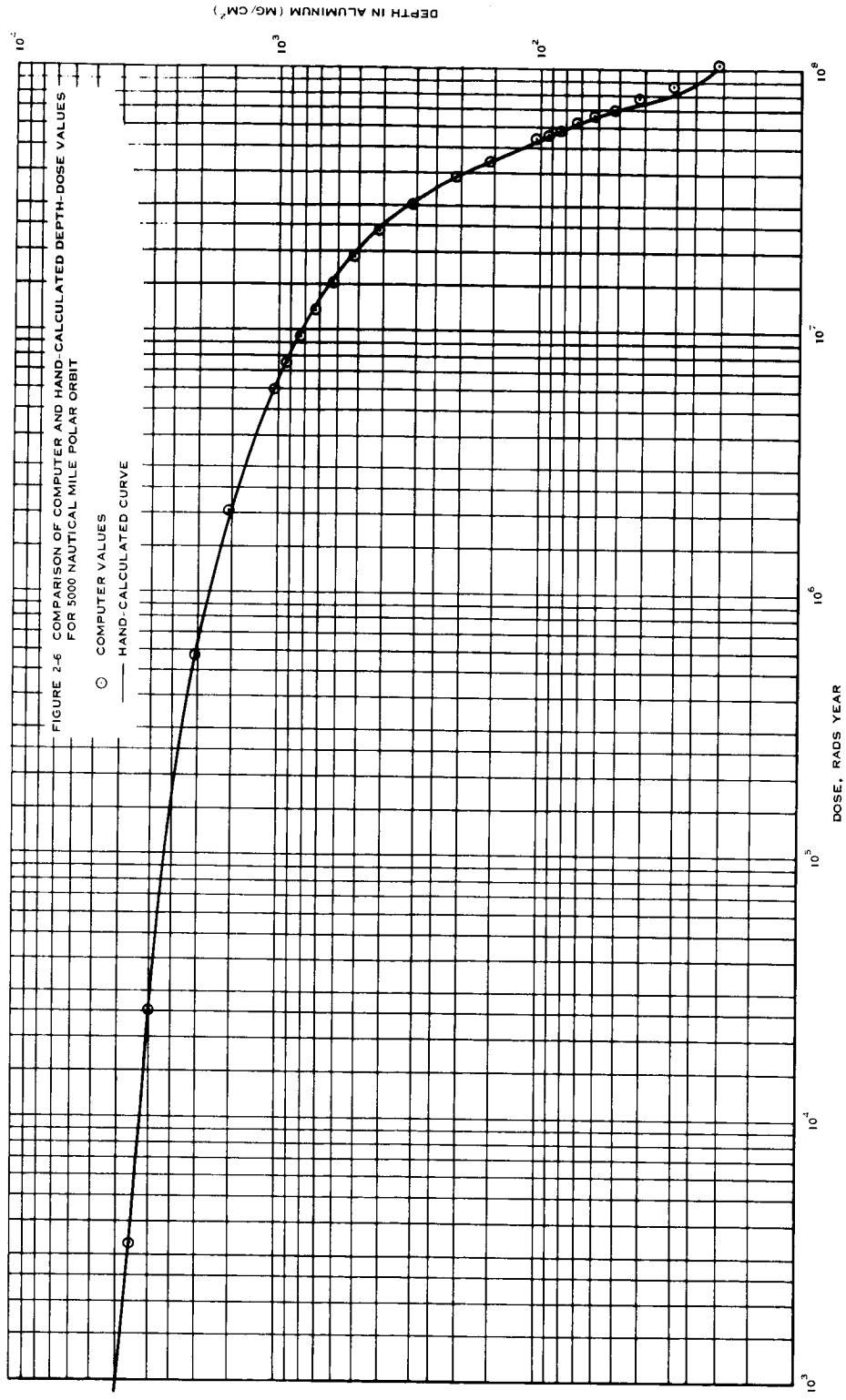
DEPTH IN ALUMINUM (MG/CM²)
10^{-1}
10^{3}
10^{2}
10^{8}
10^{7}
10^{6}
10^{5}
10^{4}
10^{3}
DOSE, RADS YEAR
FIGURE 2-6 COMPARISON OF COMPUTER AND HAND-CALCULATED DEPTH-DOSE VALUES FOR 5000 NAUTICAL MILE POLAR ORBIT
COMPUTER VALUES
HAND-CALCULATED CURVE

was used to calculate depth versus dose for a density of 4.7 g/cm^3 (Z-93 paint) for the Philco-Ford Simulator, for an 800 N. Mi. equatorial orbit and for a 1,500 N. Mi. equatorial orbit. The three output curves are presented in Figure 2-7. Derivation of the equations, an input collection and output format, and calculated results for various orbits and the Sr^{90} chamber are presented in subsequent paragraphs.

The dose/depth subroutine addition to Philco-Ford's COMPOSER (Computer Processing of Space Environmental Radiation) program performs the calculation of electron energy deposition layer by layer in an irradiated sample. The non-linear loss of electron energy over the range of its penetration is considered, and contributions from all incident energy groups are summed in each layer of interest. Bremsstrahlung and back-scattering are not considered here. This calculation is the computerization of a hand calculation developed at Philco-Ford in 1964.

The general approach implemented utilizes data from Ref. 11 which has been replotted in Figure 2-8 to express dose multiplier vs. range fraction. Range fraction is found by dividing the electron range (for any given energy) into fractions from zero (0) to one (1) wherein one (1) is equivalent in path length to the full electron range for that energy. Range fraction is obtained by converting incident electron energy to its corresponding maximum range in the material and dividing by actual penetration distance as a function of dose fraction. This maneuver combines the collection of many mono-energetic curves into one general range-fraction curve. The resulting dose multiplier has excellent agreement with the data in Ref. 11 between 0.5 and 5.1 Mev.

The composite dose multiplier M, vs. range fraction F, curve is now fit with a closed function and normalized:

$$M = 1.79 \cos^2(F-0.31)\frac{\pi}{2} - 0.37$$

and

$$\int_0^1 MdF = 1$$

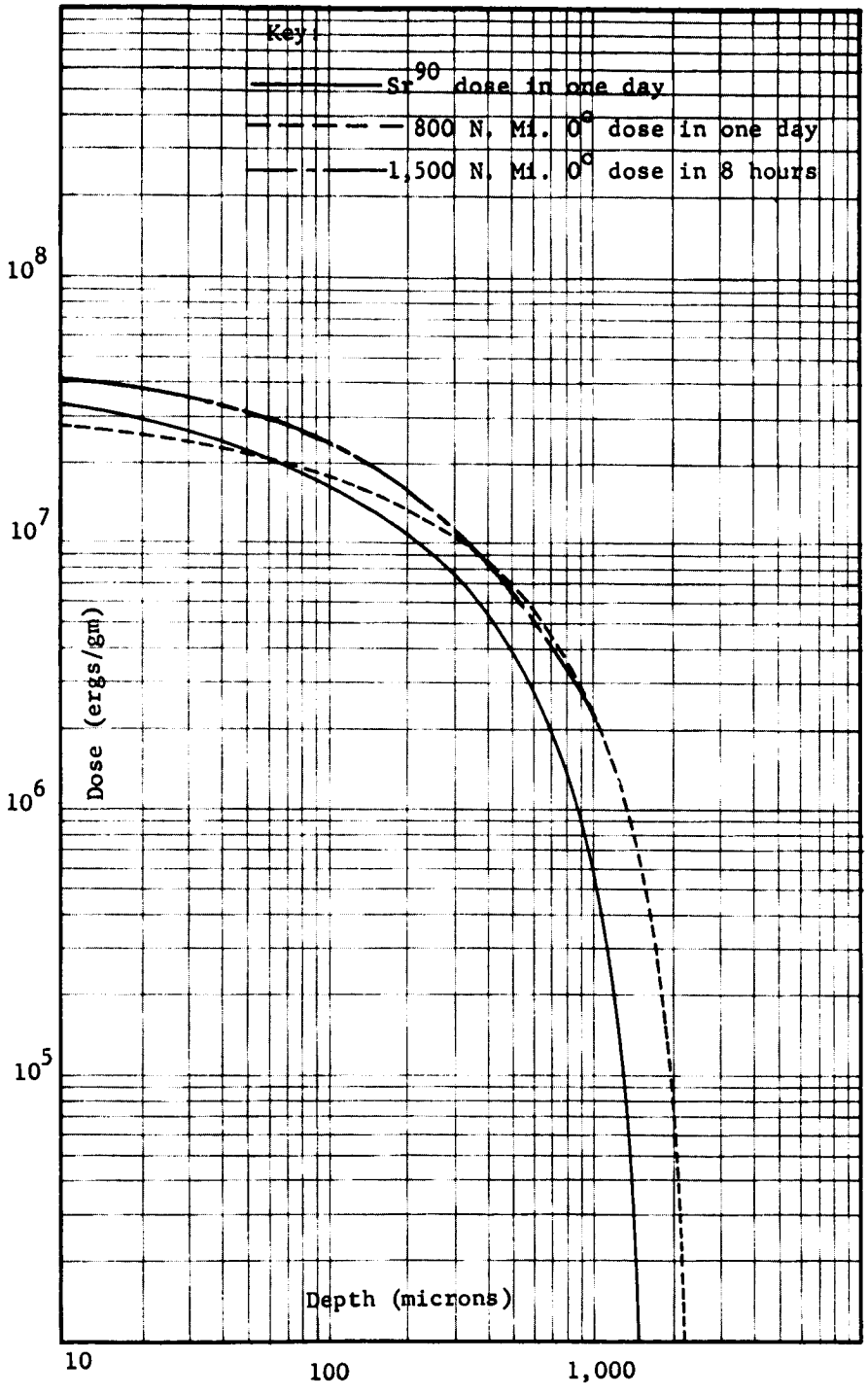

Figure 2-7 Depth Versus Dose for 4.7 g/cm^3 Paint (Z-93

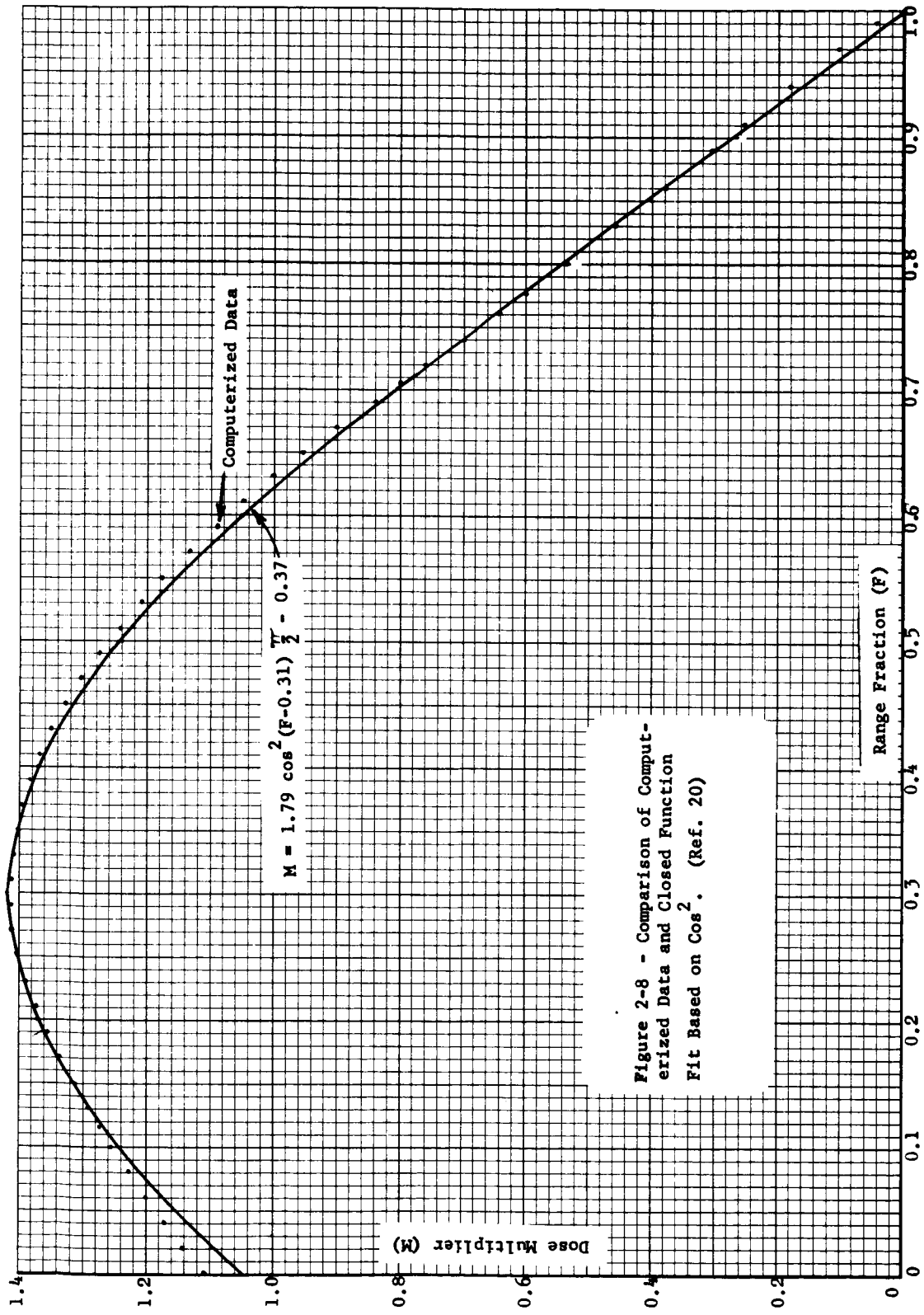

Figure 2-8 - Comparison of Computerized Data and Closed Function Fit Based on Cos^2. (Ref. 20)

The sample under irradiation with N electrons/cm^2 at energy E is divided into H regions of uniform density, ρ_h, and thickness t_h. The radiation is considered incident on the region h = 1 and penetrates sequentially into regions of ascending values of h. We wish to determine the energy deposited in any region, h_o.

From the arrangement of layers, region h_o has a front boundary (facing the radiation source at thickness, t, within the sample, and a back boundary at thickness t', where

$$t = \sum_{h=1}^{h_o-1} t_h$$

$$t' = \sum_{h=1}^{h_o} t_h$$

Similarly, the front and back "range" limits of region h_o are

$$R = \sum_{h=1}^{h_o-1} t_h \rho_h$$

$$R' = \sum_{h=1}^{h_o} t_h \rho_h$$

The incident electron energy, E, has a range, R(E), associated with it, which can be calculated from Flammerfeld's (Ref. 12) formula or the data of Katz and Penfold (Ref. 13). The front and back range fractions are thus

$$F = R/R\ (E)$$

$$F' = R'/R(E)$$

The energy deposited in region h is simply the total incident energy, NE, times the appropriate dose multiplier, M, for the region.

$$E_h = NE \int_{F}^{F'} MdF$$

$$= NE \int_{F}^{F'} [1.79 \cos^2(F-0.31) \frac{\pi}{2} - 0.37]dF$$

$$= 0.285NE [1.85(F'-F) + \sin \pi(F'-0.31) - \sin \pi(F-0.31)]$$

The computer program further generalizes this result by dividing each h-region into I subregions for finer resolution of energy deposition. The spectrum of electron energies is divided into K groups each containing N_k electrons at an average energy, $\bar{E}_k$, over a given time period. The program sums the contributions of each energy group and prints out the dose absorbed in each subregion in terms of ergs/cm^2 and ergs/g, for the given time period.

SECTION 3

SPECTRAL MEASUREMENTS AND DOSIMETRY

3.1 SPECTRAL MEASUREMENT

For the measurement of the perturbed source spectrum, the detector assembly of Figure 3-1 was employed. A 5-mm thick solid-state detector was enclosed in a lead shield (to filter out lower energy bremsstrahlung) which was surrounded by a low Z shield (to minimize the production of bremsstrahlung). As seen in Figure 3-2, the detector is sufficiently removed from the source assembly that it has an unimpeded view of three source rods and a view of the fourth through the quartz feedthrough. The entrance aperture in the lead collimator subtends a solid angle of 1.2×10^{-4} steradians from the nearest point on the quartz rod, and the collimation is obtained from the 1.4-mm diameter aperture in the lead collimator and a 1-mm thick tungsten alloy washer on the inner face of the beryllium shield.

The theoretical unperturbed spectra for two unique, first-forbidden beta emitters with 0.345 and 2.284 Mev endpoints were shown in Figure 2-3. Recent measurements (Ref. 14) have shown that the experimental spectrum closely approximates this theoretical shape. The electron spectrum obtained with the Philco-Ford detector is shown as the lower curve of Figure 3-3, while the upper curve of this figure includes the energy spectrum of gammas from bremsstrahlung originating in the source rods, chamber walls, detector assembly, etc. The energy resolution of the detection system was about 35 Kev for these measurements, as determined from the spectrum of Bi^{207} electrons. The lower curve of Figure 3-3 was obtained from the upper curve by subtracting the pure gamma spectrum obtained with a Be plug inserted into the aperture in the Be shield of the detector assembly.

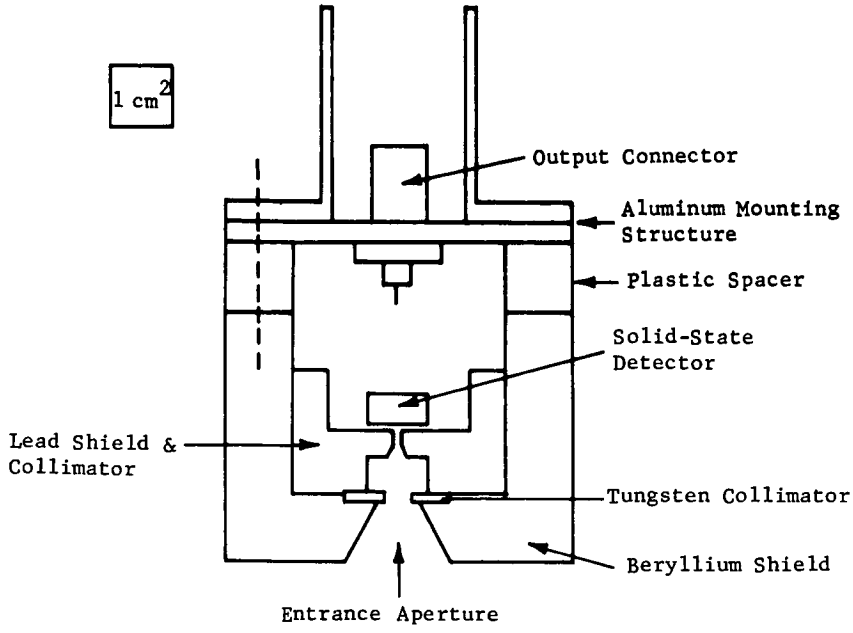

Figure 3-1 Detector Configuration for Spectral Measurement

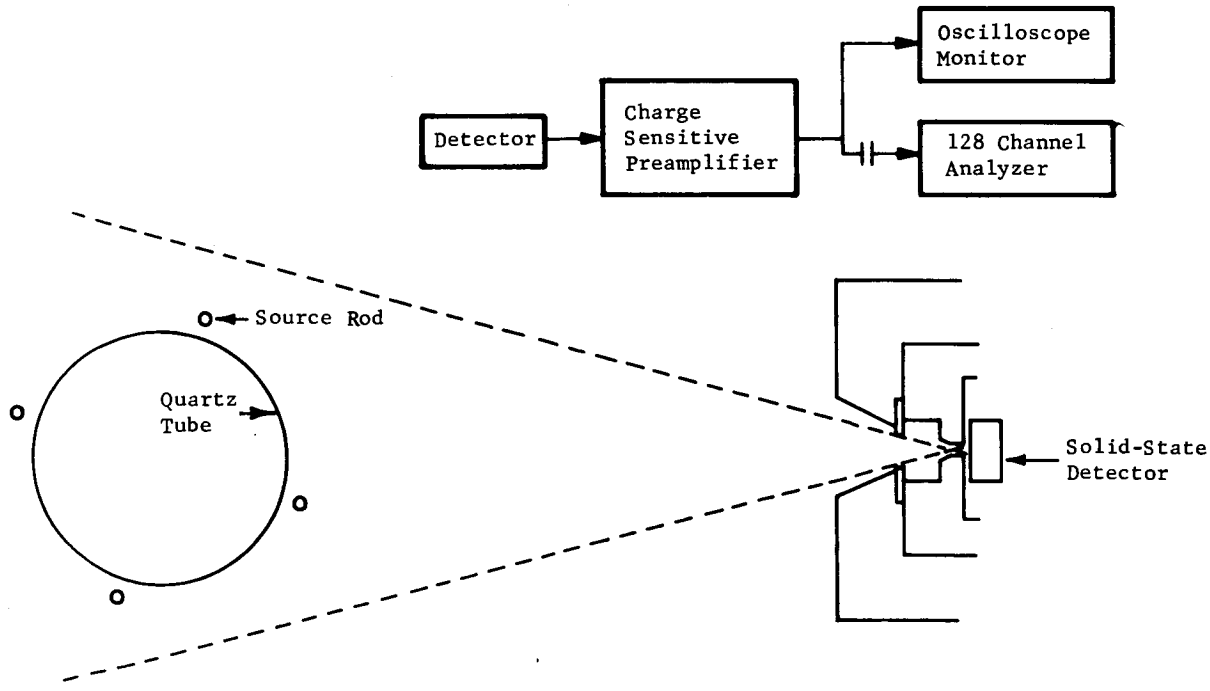

Figure 3-2 Experimental Assembly for Spectral Measurement

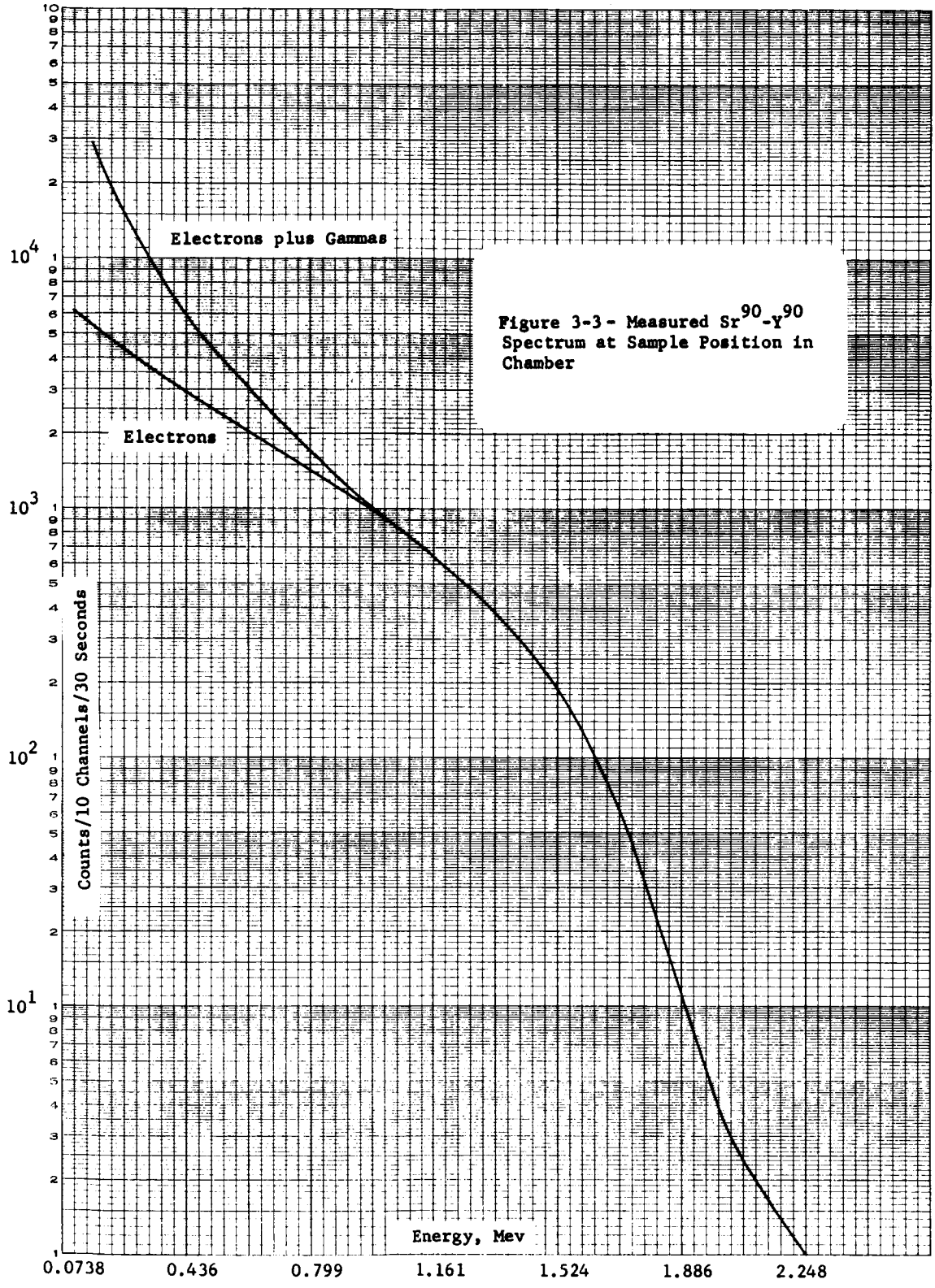

Figure 3-3 - Measured Sr^{90}-Y^{90} Spectrum at Sample Position in Chamber

3.2 THEORETICAL SPECTRUM

The Philco-Ford COMPOSER shielding program was adapted to a calculation of the theoretical perturbed Sr^{90} -Y^{90} spectrum emitted from the source rods. (Ref. 15) Shielding consisted of a stainless steel wall 0.005" thick and self-shielding within the $SrTiO_3$ filler. Each source rod was divided into 80 equal volumes and the 4π shielding was computed for each. The resultant theoretical perturbed electron spectrum between 0.3 and 2.3 Mev is presented in Fig. 3-4.

Two principal factors are responsible for the difference between the experimental spectrum (Figure 3-3) and the theoretical perturbed spectra (Figure 3-4): The first is ionization energy loss, nuclear scattering, and straggling in the source rods. The latter two effects cause a systematic low-energy "tail" to the spectrum of electrons emerging from a moderator irradiated with monoenergetic electrons, in effect causing "pile-up" of low energy electrons and a steeper spectrum (Ref. 16). The second is scattering from the surface of the quartz and chamber walls. This effect is greater for the lowerenergy electrons, and should also steepen the spectrum (References 17 and 18).

In view of the apparent error in the theoretical spectrum, the details of the computer code are not included in this report. Further work with the code is necessary to correct the sources of omission. It is believed that two or three iterations could bring the code into close approximation with the experimental results. When that point is reached, the code can be used for predicting the perturbed spectra for many variations in the source rod design and input spectra with very little effort. This can aid the generation of additional spectral matches.

3.3 SPECTRAL MATCH

The spectral match of the Philco-Ford Sr^{90} -Y^{90} perturbed spectrum with four different equatorial orbit electron spectra are presented in Figures 3-5 through 3-8.

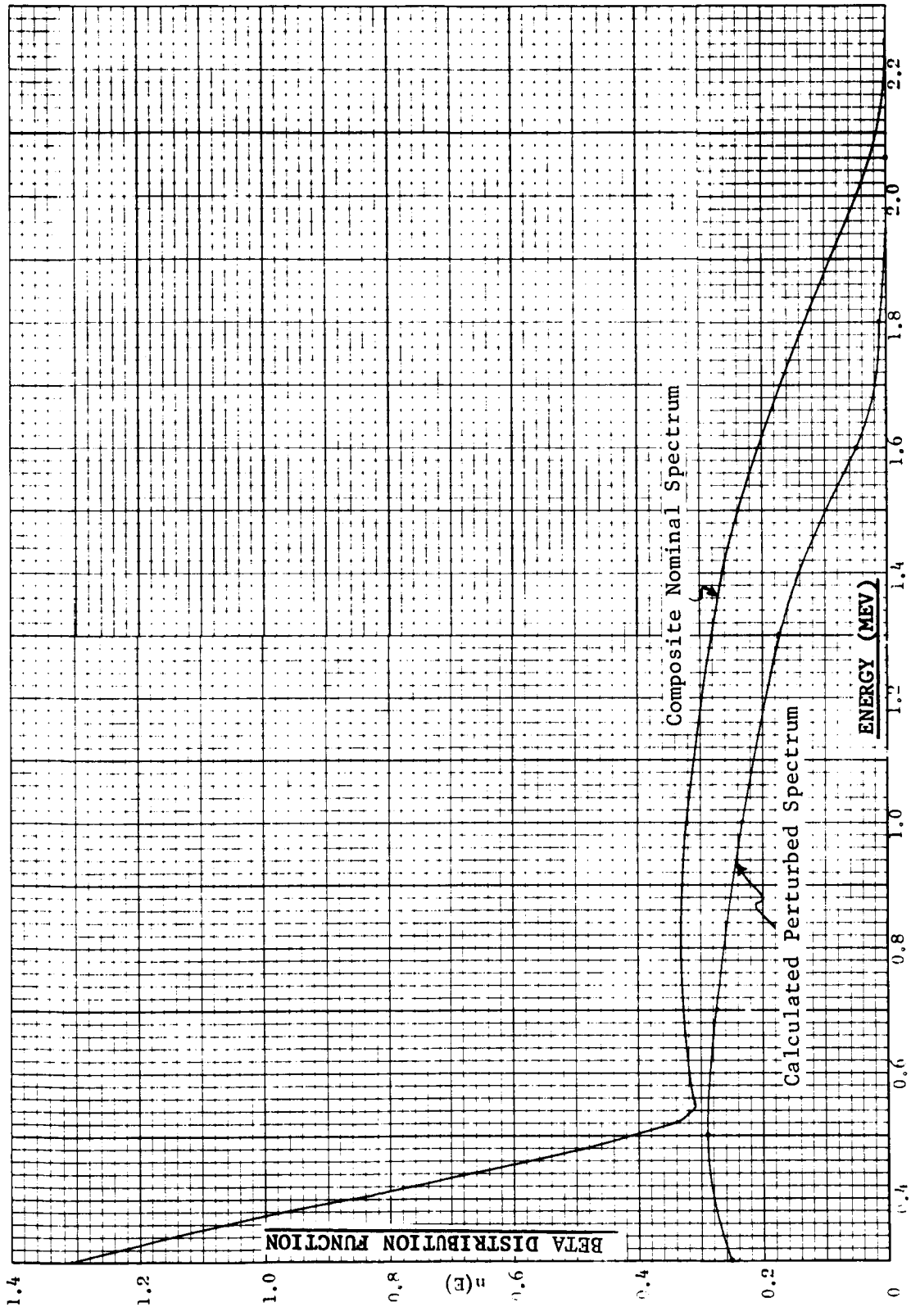

Figure 3-4 Comparison of Nominal and Perturbed Beta Spectra

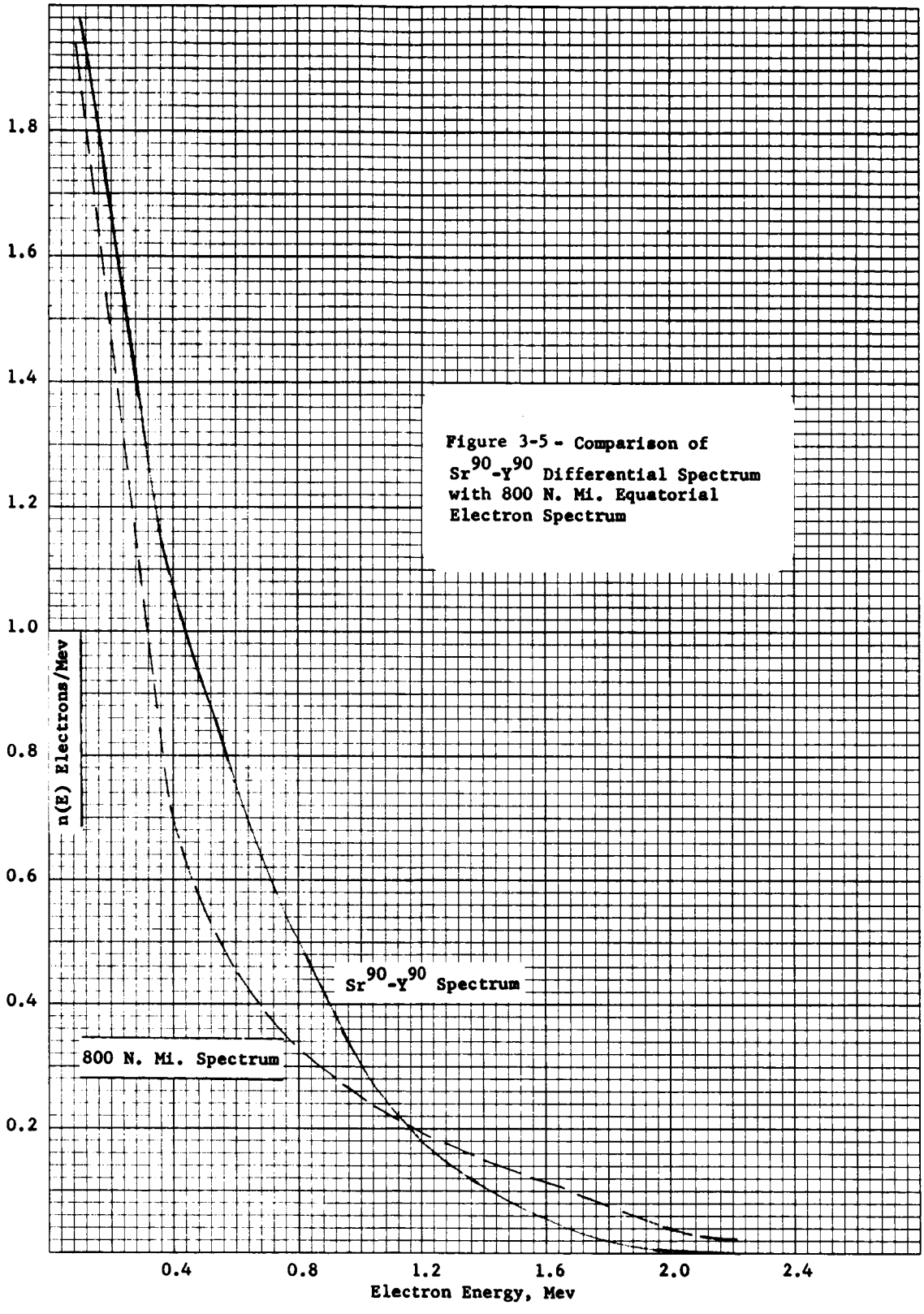

Figure 3-5 - Comparison of Sr^{90}-Y^{90} Differential Spectrum with 800 N. Mi. Equatorial Electron Spectrum

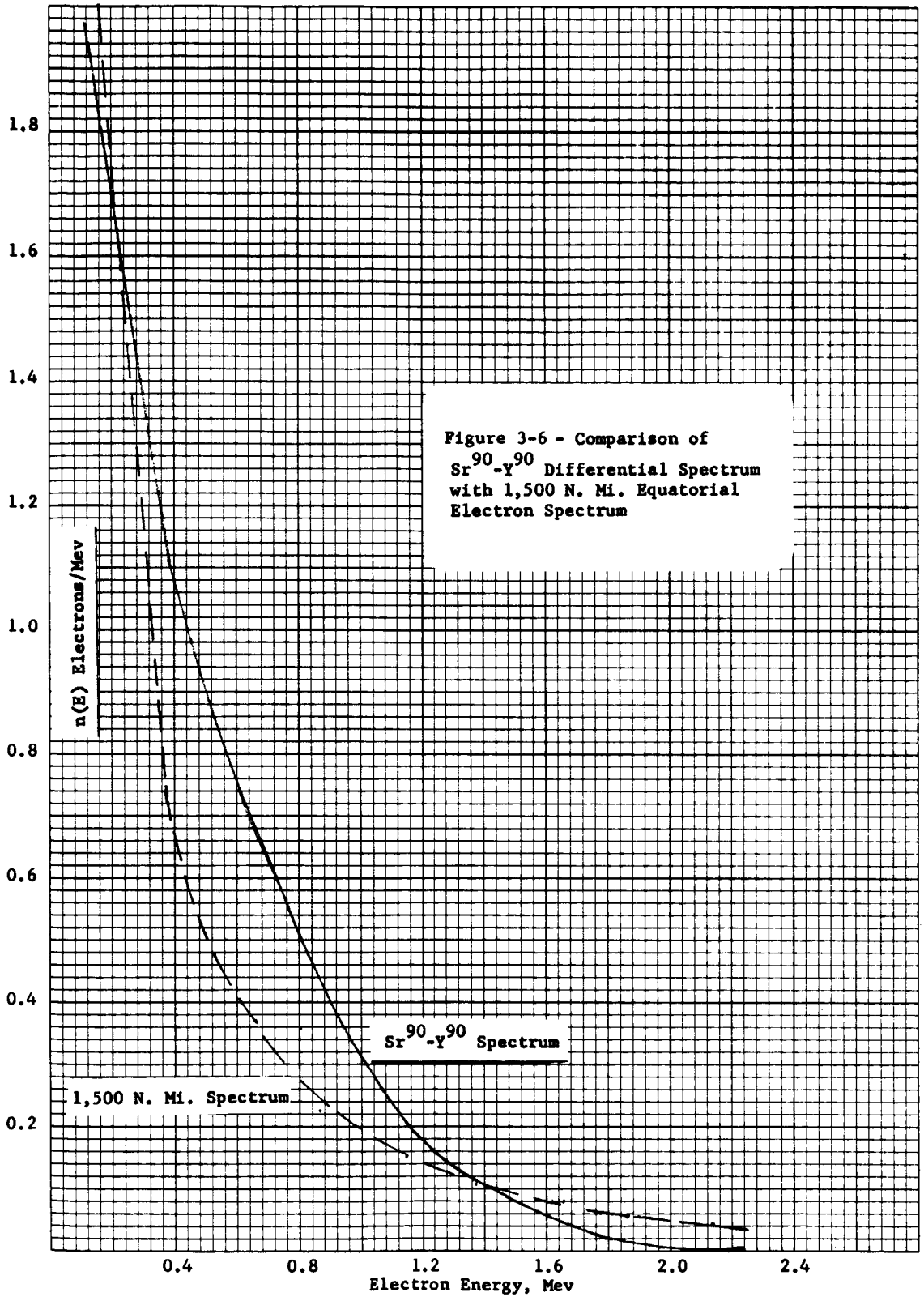

Figure 3-6 - Comparison of Sr^{90}-Y^{90} Differential Spectrum with 1,500 N. Mi. Equatorial Electron Spectrum

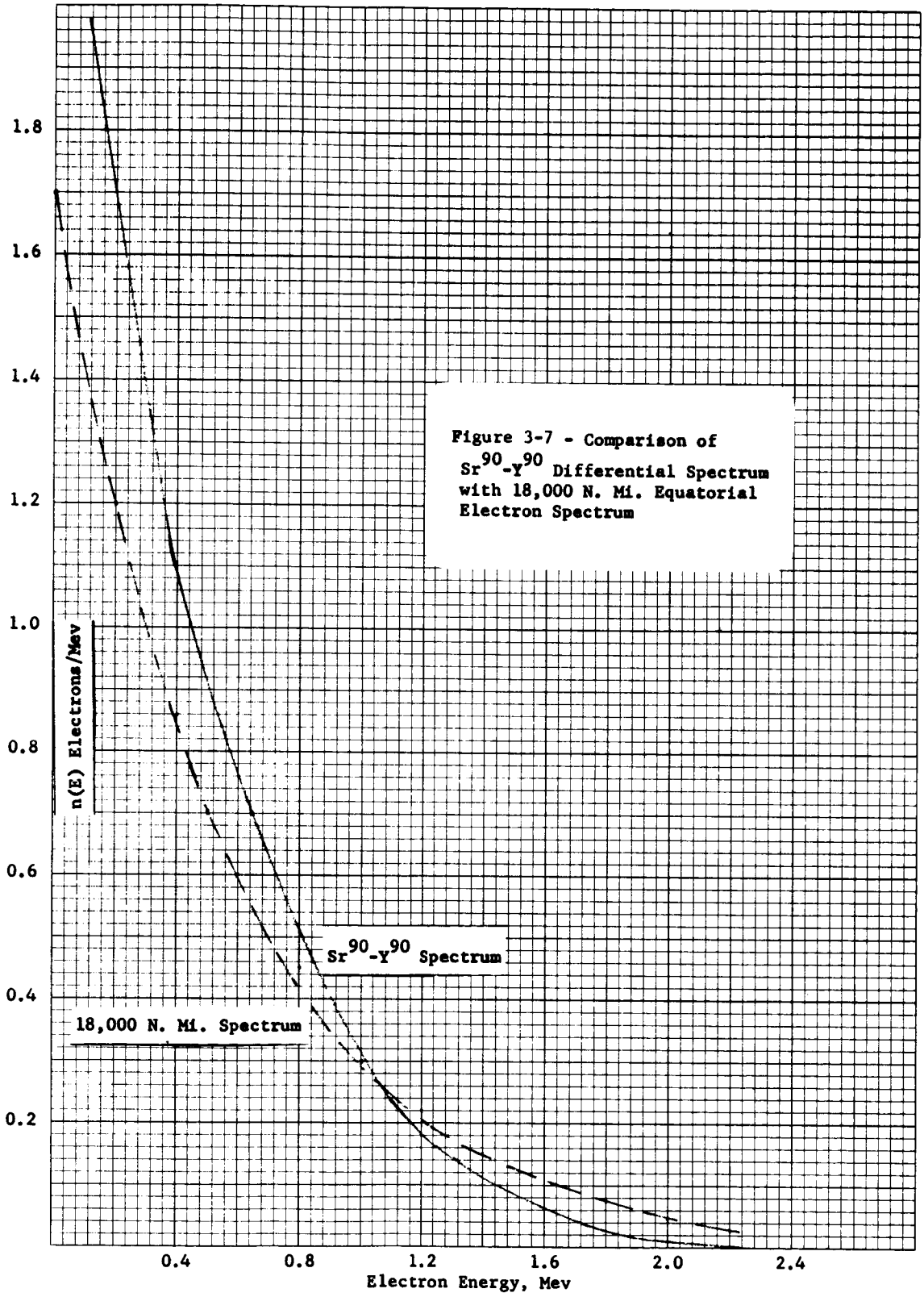

Figure 3-7 - Comparison of Sr^{90}-Y^{90} Differential Spectrum with 18,000 N. Mi. Equatorial Electron Spectrum

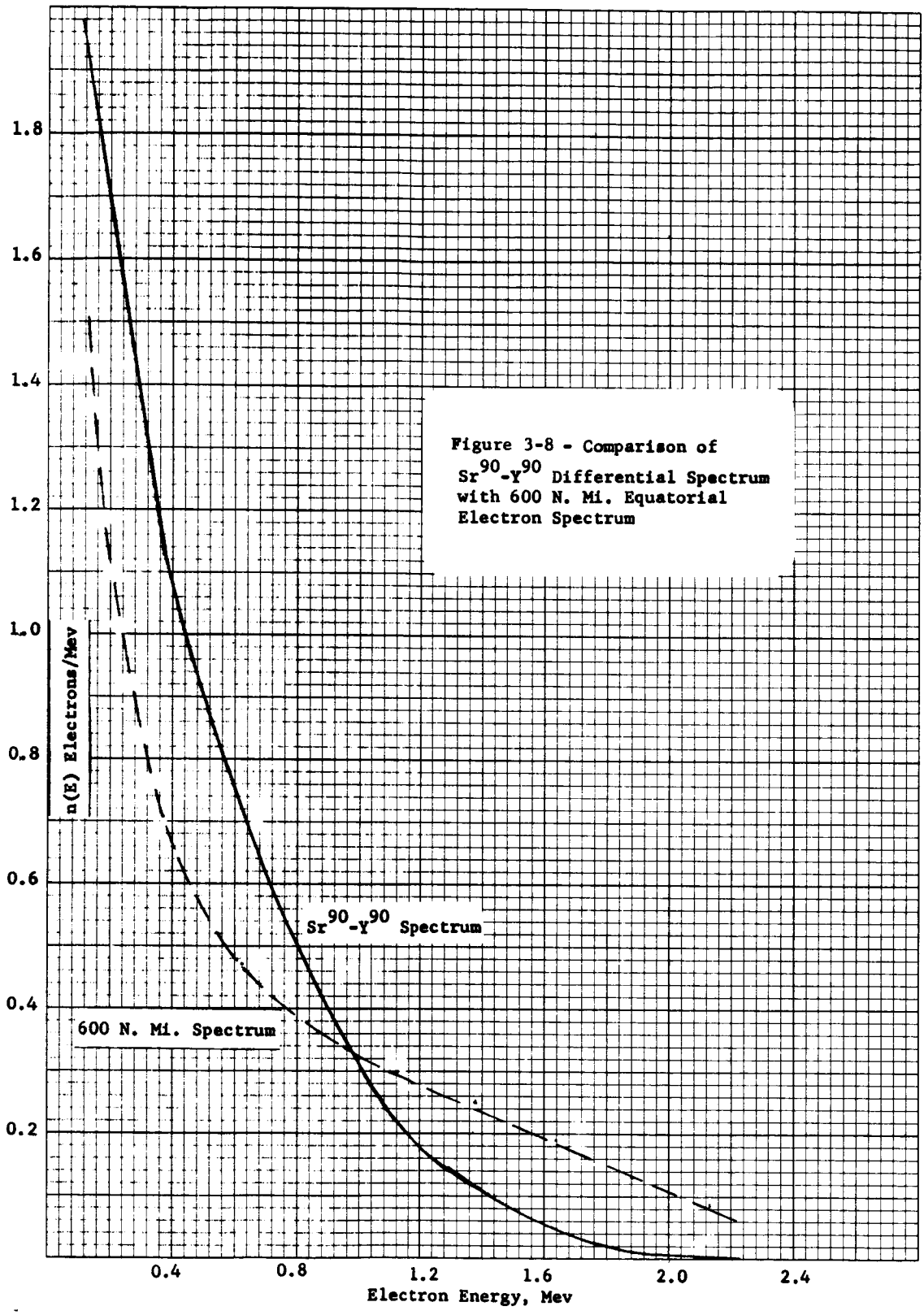

Figure 3-8 - Comparison of Sr^{90}-Y^{90} Differential Spectrum with 600 N. Mi. Equatorial Electron Spectrum

Comparisons are made of electron energy versus the normalized distribution function in terms of electrons/Mev, up to 2.24 Mev. The area under any energy band will give the fraction of the total number of electrons with those energies. This allows direct comparison of the spectra on an energy basis.

While there is no perfect match to orbital spectra, the match is quite good between Sr^{90} -Y^{90} and the 800 N. Mi. and 1,500 N. Mi. orbits, particularly at the lower energies. The match is poorest in the region between 0.4 and 0.8 Mev, where there are too many electrons in the simulator, and at the highest energies, where the simulator is deficient in electrons. At the energy of greatest deviation, the orbital requirement is within 54 percent of those provided by the simulator. These are considered satisfactory matching spectra.

A fairly good match is also found with the 18,000 N. Mi. spectrum. In this case, the greatest deviations occurred at the lowest energies. In the energy bracket 0.12 to 0.16 Mev, the orbital requirement was 70 percent of those provided by the simulator.

The 600 N. Mi. spectrum deviates excessively at both low and high energies.

No other comparisons have been made, but it is possible that many good spectral matches exist beyond those mentioned here. Both inclination and orbital distance must be considered in the comparisons.

A good simulation requires consideration of the flux as well as a spectral match. In order to avoid excessively long irradiation, it was desirable to select a flux close to the peak of the Van Allen Belts. This was done, and the flux at the 5-inch sample position is superimposed on a plot of the equatorial orbit flux in Figure 3-9. The measurements and calculations used to determine this flux are described in Section 3.4.

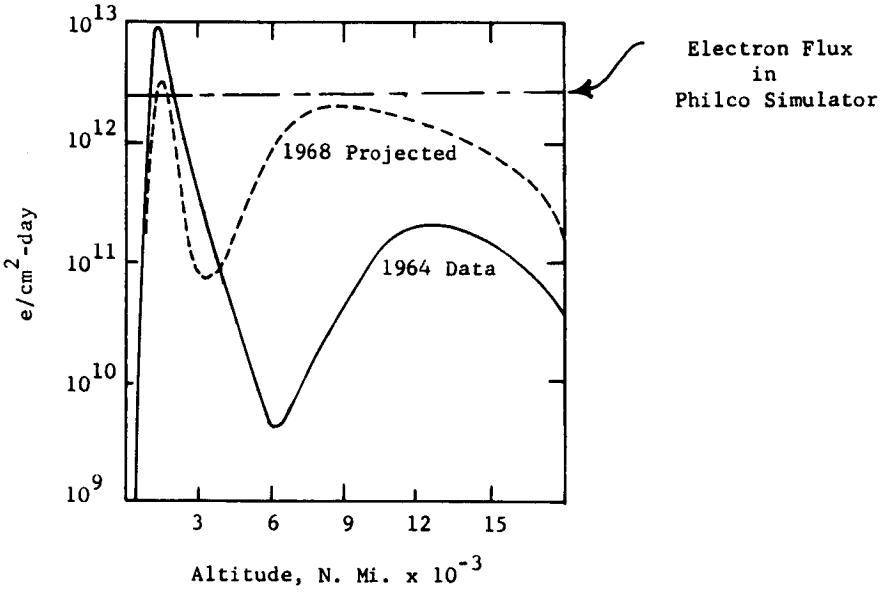

Figure 3-9 - Comparison of Electron Flux in Philco Simulator and Orbital Fluxes at 0° Inclination (Ref. Vette, J. I., NASA SP-3024)

3.4 DOSIMETRY AND ELECTRON FLUX

3.4.1 Dosimetry

Two dosimetry techniques were used. They were: Thermoluminescent Dosimetry (TLD), using 5 mil thick discs of lithium fluoride-impregnated Teflon; and Cellophane Dosimetry, using three layers of E.I. du Pont MSC 300 dark blue cellophane, one mil thick. Both dosimeters were backed by aluminum to approximate the backscattering in thermal control sample substrates.

Each type of dosimetry involved two steps: (1) calibration with Co^{60} gammas, and (2) mapping 10 sample positions in the vacuum chamber.

Difficulty in the reproducibility of TLD dosimeters was overcome by selection of uniform weights of discs. The Co^{60} calibration precision improved to ±20 percent, which is in the same magnitude as reported by other workers for Teflon disc dosimeters (Ref. 19). Table 3-1 lists the results of the measurements, with precision values given at the 95 percent confidence level.

TABLE 3-1
CHAMBER DOSIMETRY AND Co^{60} CALIBRATION

Description	TLD	Blue Cellophane
Average sample dose rate in chamber, rad/hr	3.0×10^3	4.3×10^3
Precision of chamber measurements	±20.5%	±16.3%
Precision of Co^{60} calibration measurements	±20.4%	±50%

The sample size for chamber measurements was one per position for both types of dosimetry. Sample size for the Co^{60} calibrations was 10 per dose for two doses (TLD) and one per dose for four doses (cellophane).

As can be seen in Table 3-1, all precision values were quite satisfactory, except for the Co^{60} calibration of cellophane. The calibration curves are presented in Figure 3-10 and Figure 3-11. The shape of the TLD calibration curve has been firmly established by the past history of many calibrations. Therefore, only two dose points were used to calibrate the dosimeters used in the contract.

The poor calibration precision for the cellophane is attributed to variations in the moisture and/or air content of the cellophane during Co^{60} irradiation. Previous workers have found the same problem (Ref. 20 and Ref. 21).

Young (Ref. 21) found that moisture content and film batch can cause up to a factor of six change in slope of the calibration curve. In the current contract work, both desiccated and evacuated vials were used. Pressure could not be monitored on the evacuated vials, and the actual pressure during irradiation was not known. The vials were copper tubing, pinched off after a brief pump down to 10^{-7} Torr. The evacuated vials yielded results which ranged from a slope comparable to that for the desiccated vials to a slope which gave a dose rate (for the sample position in the chamber) exactly the same as the TLD dosimetry, 3.4×10^3 rad/hr. However, there was no justification in accepting either value alone and the best estimate of the slope was obtained unbiased from all of the vacuum data. Conversion from Co^{60} roentgen to rads was made by multiplying by 0.877. This is the conversion factor for roentgen air dose to rads of energy deposited in carbon.

Fortunately, the actual chamber position mapping precision was much better than the Co^{60} calibrations. Here, all ten samples of blue cellophane were exposed to identical conditions; 500 hours of chamber evacuation at 1×10^{-6} Torr, followed by a day of equilibration to room air conditions. This gave the excellent precision for sample positions of $\pm$ 0.7 x 10^3 rads/hr for the blue cellophane and $\pm$ 0.6 x 10^3 rads/hr for the TLD dosimetry. This amounts to $\pm$ 16 percent for the former method and $\pm$ 20 percent for the latter, on the 95 percent confidence level.

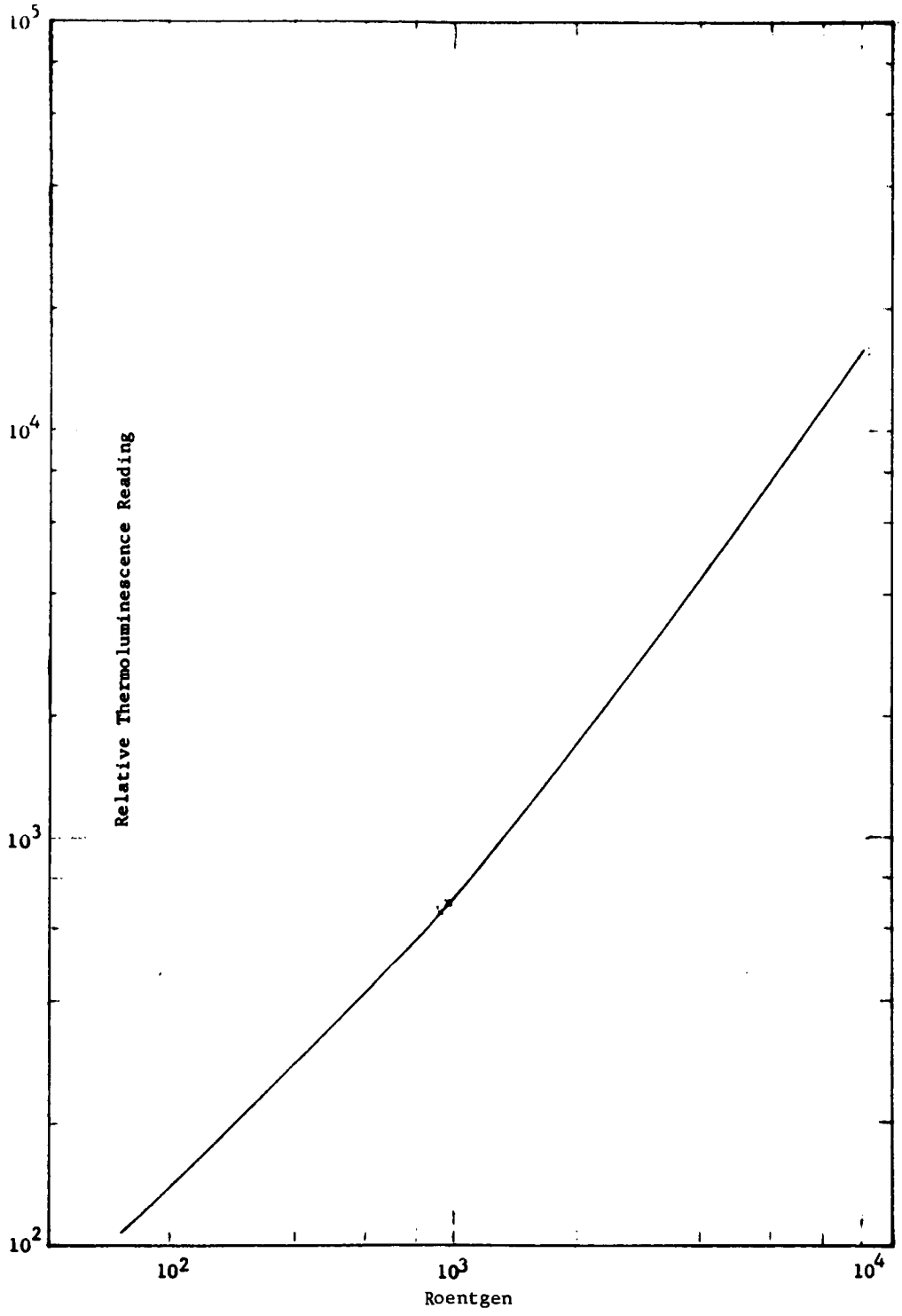

Figure 3-10 Thermoluminescence Calibration

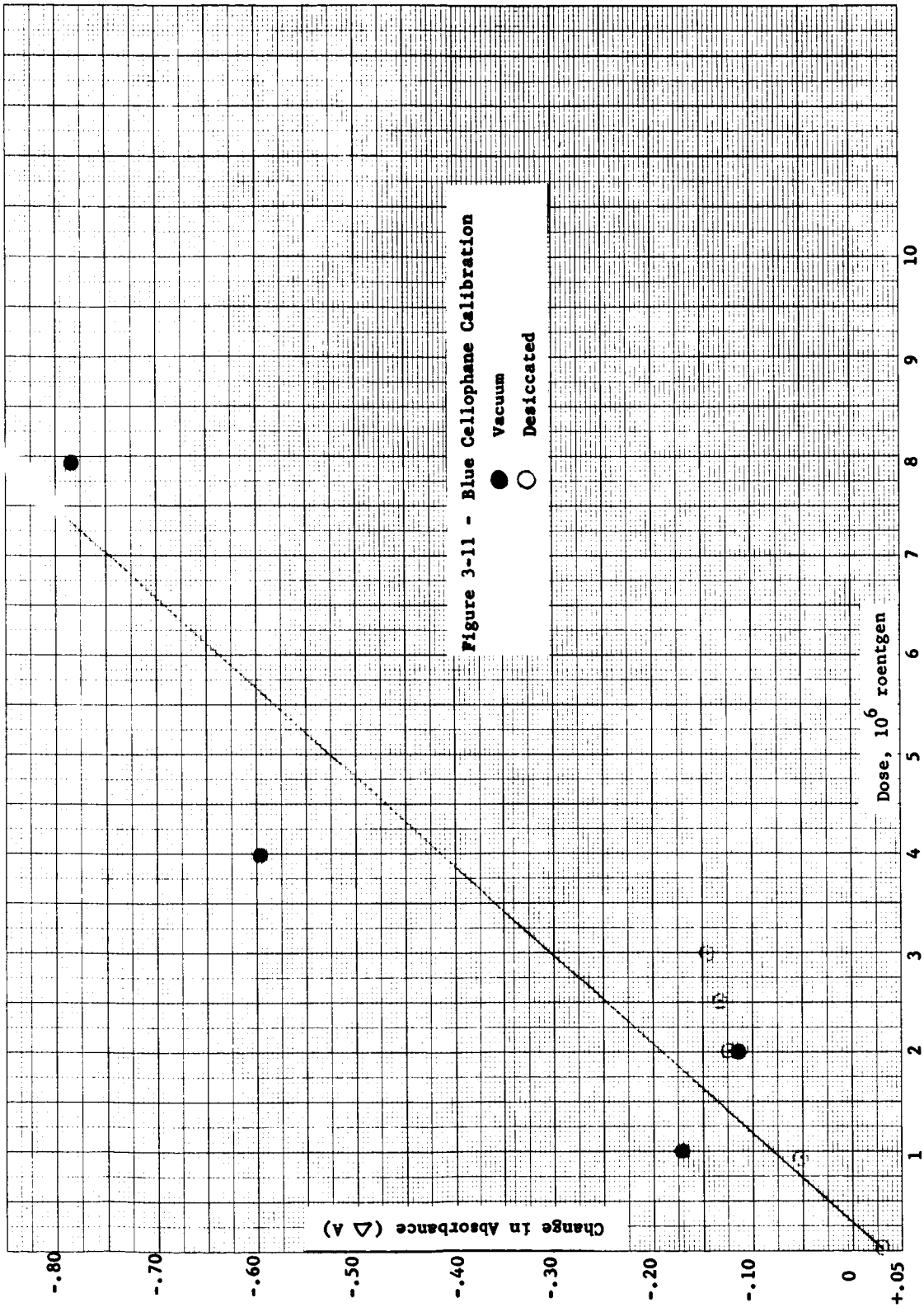
Figure 3-11 - Blue Cellophane Calibration
Vacuum
Desiccated
Change in Absorbance (Δ A)
-.80
-.70
-.60
-.50
-.40
-.30
-.20
-.10
0
+.05
Dose, 10^6 roentgen
1
2
3
4
5
6
7
8
9
10

Mapping of the sample positions is presented in Figure 3-12. Only one position was out of the 95 percent confidence limits; this being position 9 for blue cellophane. The TLD value was not comparably high, therefore, there is no justification in using a higher dose rate value for this position than for the others. Since the chamber-mapping precision and the Co^{60} calibration precision were the same ($\pm$ 20 percent) for TLD, there is no statistical justification in assigning different dose rates to any of the sample positions. The average value will therefore be used for all sample positions.

The spread of 1.3×10^3 rads/hr. between blue cellophane and TLD is not desirable and a better calibration may bring them closer. The calibrations assume absolute flatness of response with energy and no linear energy transfer effects (LET) in either response or readout, and this is most certainly not the case. Back-scattering by the aluminum (up to 10 percent) will even out some of the LET differences, but even here the TLD dosimeters are thicker (5 mils as opposed to 3 mils) than the blue cellophane dosimeters. An attempt was made to determine LET effects on the blue cellophane by measuring separately the absorbance of each of the three layers compromising each sample. (This measurement would make use of the extinction coefficient k for the equation $\frac{I}{I_0} = e^{-kt}$, where t is the film thickness.) However, all three layers had the same absorbance, indicating (within measurement capability) no dose-depth variation for the first three mils of blue cellophane.

A theoretical evaluation of the dose rate or flux distribution at several distances from the source has been made (Appendix B). This evaluation indicated a slightly higher dose rate for the sample positions which were looking at three source rods, as opposed to those positions looking at only two source rods (See Figure B in Appendix B). This variation could not be found in the dosimetry measurements.

Key:

( ) x 10^3 rads/hr (Blue Cellophane)

[ ] x 10^3 rads/hr (TLD Dosimetry)

Average Values:
(4.3) Blue Cellophane
(3.0 TLD

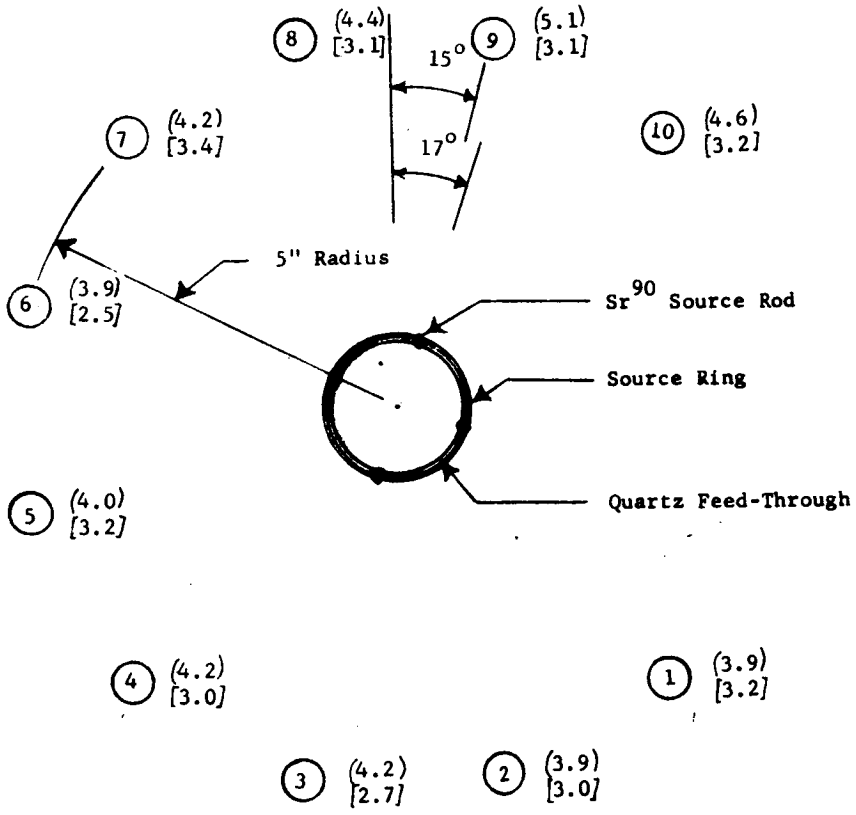

Figure 3-12 Sr^{90} Source Rod Locations and Sample Position Dosimetry Mapping

Scale: 1:2

3.4.2 Electron Flux at the Sample Position

It is desirable to know the electron flux as well as the absorbed dose rate, at the sample position. Therefore, it was necessary to calculate the flux from the experimental dosimetry. This calculation includes two sources of error which cannot be avoided: (1) dosimetry error, and (2) the presence of linear energy transfer (LET) effects in the calculated energy absorption. In spite of the presence of some error, the estimated flux numbers are of value for relating damage results and orbital simulation.

The equivalent 1 Mev flux (ϕ_1Mev) was calculated for a typical material, carbon. The conversion factor for converting the dosimetry results in rads to equivalent 1 Mev electrons was obtained from the basic equivalence of a rad (Ref. 20).

$$1 \text{ rad} = 6.25 \times 10^{13} \text{ ev/g}$$

The range of a 1 Mev electron in carbon is 0.49 g/cm^2. All of the electrons are stopped within this range, but the dose deposition is non-uniform and follows a cosine distribution function. The peak dose is approximately one-third of the maximum range. The total energy deposited is equal to the area under the depth-dose curve. The area of a rectangle obtained by assuming a constant dose deposition rate, that being the surface dose (starting point of the cosine curve). Because of the near equality of the two areas, experimental thin-film dosimetry can be used as the best approximation for converting to total energy absorbed within the range of the electrons:

$$1 \text{ rad} = 6.24 \times 10^{13} \text{ ev/g or } 6.24 \times 10^{7} \text{ Mev/g}$$

By depositing all of the energy (equivalent 1 Mev electrons) within the electron range in carbon, the energy deposited can be related to the area (2.04 cm^2) subtending a volume of carbon weighing one gram. Thus,

$$6.24 \times 10^{13} \text{ ev/g} = \frac{6.24}{2.04} \times 10^{13} \text{ ev/g or } 3.06 \times 10^{13} \text{ ev/cm}^2$$

This is rounded out to 3×10^{13} ev/cm^2 or 3×10^7 Mev/cm^2. For 1 Mev electrons, one (1) rad would be the energy deposited from a flux of 3×10^7 e/cm^2 (1 Mev).

The above conversion factor is now applied to the experimental dose measurements to determine the equivalent 1 Mev electron flux. The average dose rate for the two types of dosimeters was found to be:

$$DR = \frac{3.0 \times 10^3 + 4.3 \times 10^3}{2} = 3.7 \times 10^3 \text{ rad/hr}$$

The corresponding electron flux was:

$$\phi_{1 \text{ Mev}} = \frac{3.7 \times 10^3 \times 3 \times 10^7}{3.6 \times 10^3} = 3.1 \times 10^7 \text{ e/cm}^2\text{- sec (E} \equiv \text{1 Mev)}$$

SECTION 4

EVALUATION OF THE PROTOTYPE SIMULATION CHAMBER

4.1 CHAMBER DESIGN

The prototype chamber with the associated electron and ultraviolet sources is illustrated in Figures 4-1 and 4-2.

The prototype chamber was satisfactory for the purpose intended. There were no maintenance problems, no shut-downs, no difficulty in achieving a vacuum of 10^{-6} Torr. The chamber was successful, not only in accomplishing the goals of the prototype run, but also in pointing out deficiencies that should be corrected in subsequent chambers.

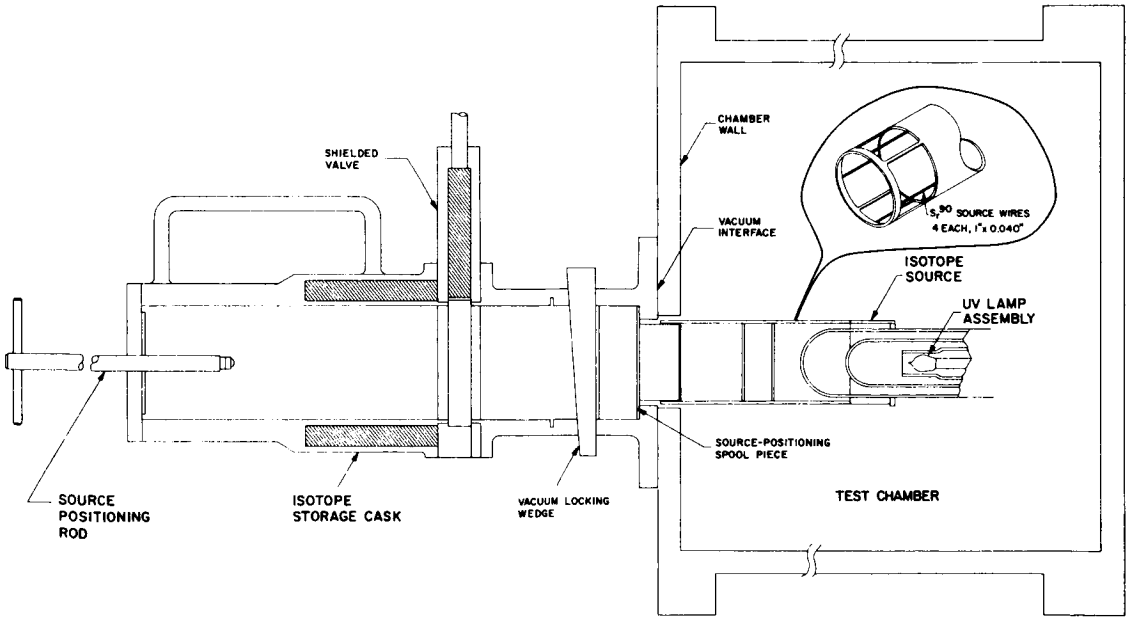

Figure 4-1 Radioisotope Source Configuration

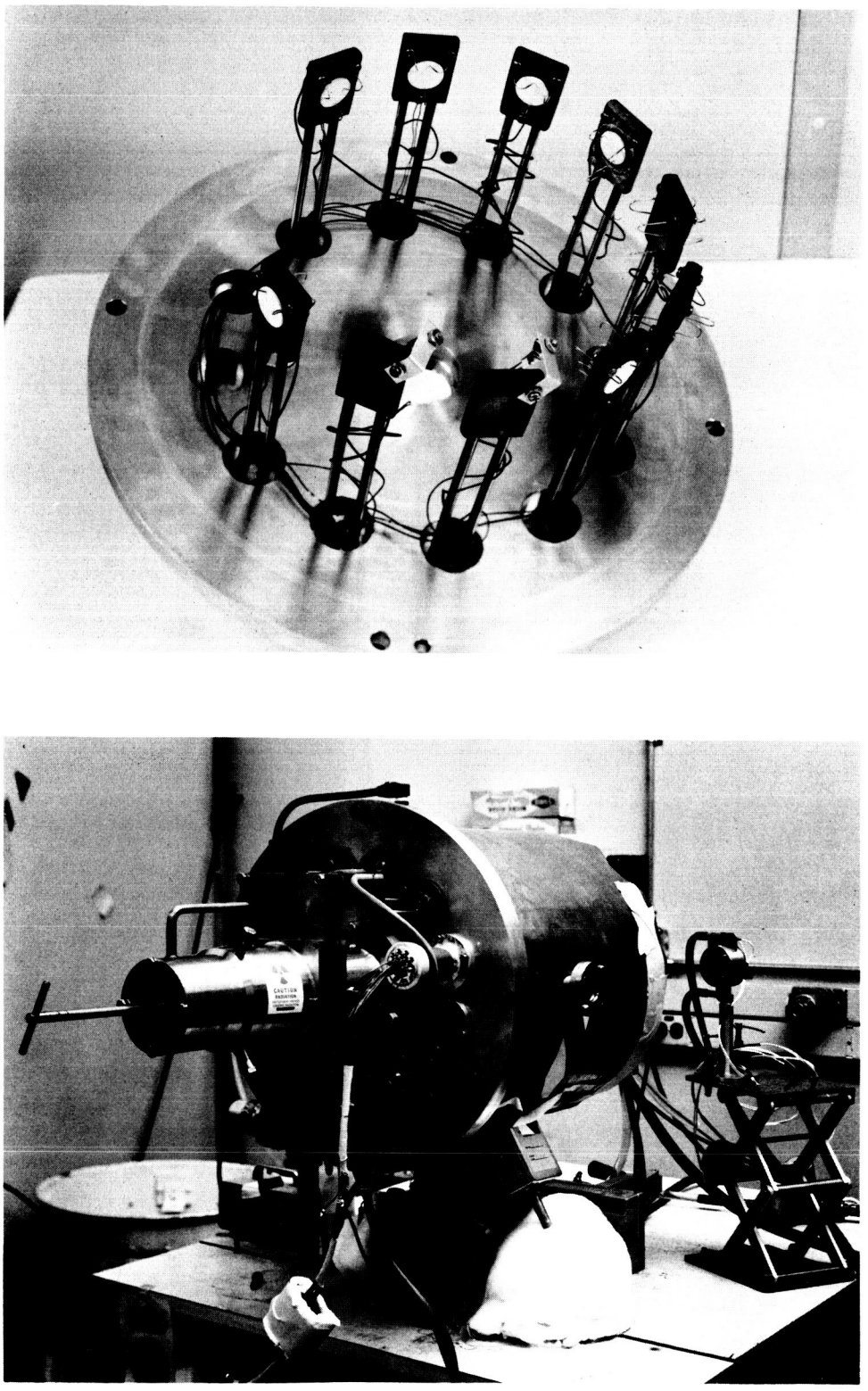

Figure 4-2 Sample Flange and Simultation Chamber

The deficiencies of the prototype chamber include the following: (1) provision for only one sample dose rate and one ultraviolet exposure rate, (2) too small a number of sample positions (ten), (3) no in situ capability for optical measurements (except for monitoring the ultraviolet output), (4) a contamination potential when used for optical materials. No oil could be identified inside the chamber after the run; however, backstreaming is always a consideration in oil-diffusion pumped systems. Liquid nitrogen trapping was used during the run; however, the trap was inadvertently empty for short periods six times during the test period due to failure of the liquid nitrogen supply system. The total empty time did not exceed a few hours; nevertheless, this was a highly undesirable occurrence.

Three other sources of contamination were found in the chamber. The first was tungsten oxide, deposited in the vicinity of the nude gage tube, formed when a gage filament was inadvertently burned out just prior to the start of the prototype test.

The second additional source of contamination was of the radioactive type. Five samples were slightly contaminated. They were as follows:

A1-4 - 1,000 decompositions/minute (d/m)
A3-1 - 50 d/m
A3-2 - 50 d/m
A4-1 - 55 d/m
A4-2 - 100 d/m

Identification of the samples is given in Section 5. The radioactivity is given in decompositions/minute, obtained by multiplying the counting rate by the machine geometry. This contamination appears to derive from small amounts of brazing flux which had trapped traces of $SrTiO_3$ during welding of the source rods in a hot cell. This much physical contamination, if present as pure $SrTiO_3$, could not contribute to changes in the optical properties of the coatings. Based on the maximum contamination of

1,000 d/m in a 10 micron layer of coating material of density 4.7 g/cc, the contamination would amount to only 0.035 ppm (35 parts per billion), an insignificant amount.

The contamination levels were within the values allowed by the California State Atomic Energy Commission for sealed sources, and according to California standards, there is no evidence of a leaky source. The allowable limit, by definition, is 0.005 microcuries of loose contamination. This amounts to 11,100 d/m as calculated by the equation:

$$0.005 \text{ uc} \times 2.2 \times 10^{6} \text{ d/m-uc} = 11{,}100 \text{ d/m}$$

Since May 1966, contamination levels have dropped to zero. In the prototype run, slight contamination again appeared, probably because of the long run time and continuous heating by the ultraviolet source.

The third additional source of contamination was a small amount of visible contamination of some type on the quartz finger, underneath the shadow of the source holder. This was a fine material, easily removed, and was not radioactive. The source of this contamination could not be identified, although it could have been oil, and the apparent deposition pattern remains unexplained.

The sample temperature control system (large water tank and pump) would not be satisfactory for a permanent system. Thermoelectric or resistance heaters are the only satisfactory method of temperature control for several different sample temperatures. These will be incorporated, where possible, in future designs.

The only disadvantage of the prototype source assembly was related to the vacuum-seal design. The source cask was designed (because of cost factors) such that the source rods have to be inserted into the chamber before the vacuum seal is made. Likewise, the vacuum seal is automatically broken at the time of source removal. Advanced design source assemblies will correct this deficiency.

4.2 RADIATION SHIELDING AND SAFETY

A combination of 0.1875 inch steel and 0.0625 inch lead was more than sufficient shielding for safe operation of the radiation chamber (Figure 2-5). The peak dose rate (at contact) at the side of the chamber is 170 mr/hr. Personnel exposure has never exceeded 19 mr/day since receipt of the source assembly. The average daily exposure with considerable work going on is 2 mr/day, far below the Atomic Energy Commission's allowable values.

A 0.2 micron filter was mounted on the high pressure side of the forepump. Air sampling above this filter has been continuous through every vacuum operation with the source inside the chamber, and there has been no measurable radioactivity on any air sample to date. Room air sampling at other times has likewise yielded no radioactivity.

Samples of both diffusion and roughing pump oil were taken at the conclusion of the dosimetry run and again after the prototype exposure run. These samples were filtered and the filters checked for radioactivity by the Radiation Safety Officer. No radioactive contamination was detected for any sample.

The present radiation-area control system of limited personnel access and use of film badges in the vicinity of the radiation source has proven satisfactory. Other than an annoyance factor related to the audio alarm, the system has worked satisfactorily. With continuation of the present close surveillance of the source and work area, no problems are anticipated, even with higher level sources.

4.3 ULTRAVIOLET SOURCE CALIBRATIONS

The energy produced by the AH-6 lamp was measured daily throughout the test. Measurement was made with an Eppley Thermopile, located outside the 1-inch quartz window. The energy of interest is the ultraviolet region, between 0.25 and 0.40 microns. Being a high pressure (100 atmospheres) mercury arc

lamp, the AH-6 produces more continuum between peaks than does a low pressure mercury lamp. Peaks occur at 0.25, 0.28, 0.30, 0.312, 0.335, 0.365, and 0.404 microns. Figure 4-3 shows comparisons of the AH-6 spectrum, xenon lamp spectrum, and Johnson's curve of the solar spectrum. Figure 4-4 shows the importance of pressure in the continuum part of the uv spectrum, the AH-6 output lying between the spectra at 75 and 165 atmospheres. Approximately nine percent of the total solar energy is below 0.4 microns. This amounts to approximately 12.4 milliwatts/cm^2. The water and quartz which constitute the lamp envelope, cooling system, and vacuum feed-through transmit about 60% or more of the AH-6 lamp radiation output down to 0.25 microns. The vacuum feed-through was made with GE-204 synthetic quartz. The velocity tubes and water jackets are fabricated from GE-104 or a comparable synthetic quartz.

In order to calculate the ultraviolet energy seen by the samples, the following factors were considered:

(1) Separate the ultraviolet from the other energies.
(2) Correct for sample distance versus detector distance.
(3) Correct for quartz window attenuation (quartz window in the vacuum chamber).

The essential measurements and calculations were made, resulting in the following equation for calculation of equivalent sun hours (esh) in the 0.25-0.40 micron wavelength region:

$$esh = KK^1 \text{ (5265 filter response} - 0.54 \text{ [5263 filter response])} t$$

where K = a general multiplier constant,

and K^1 = a specific multiplier constant applicable to the system and geometry.

t = time in hours

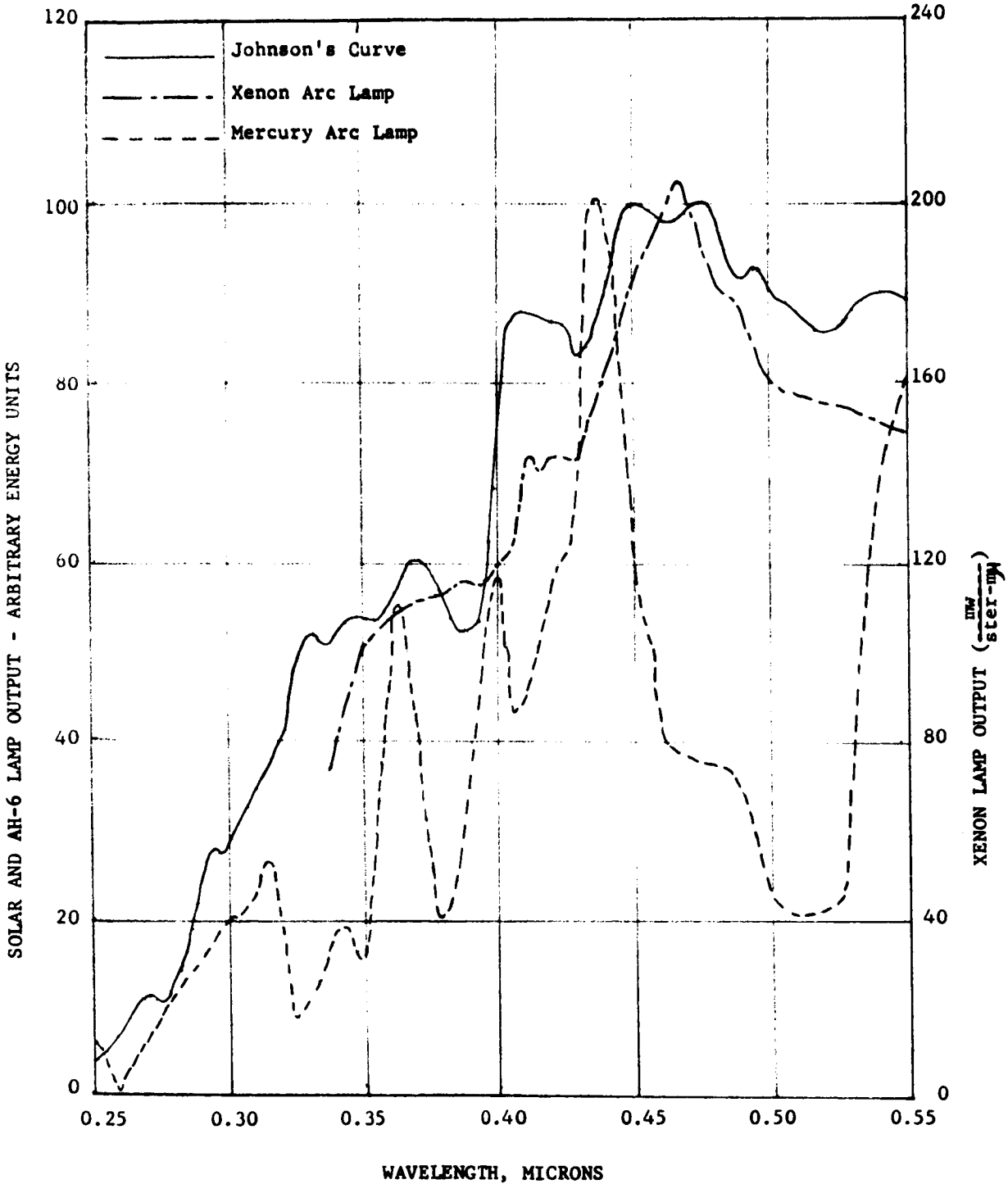

Figure 4-3 Spectral Energy Distribution for Solar, Mercury Arc, and Xenon Arc Radiation

The basis for the form of the equation and derivation of the multiplier constants K and K^1 are described in subsequent paragraphs.

Separation of the Ultraviolet Energy

Two narrow band pass filters were used to determine the spectral form of the energy output. Transmission curves of these filters were superimposed on a spectral output curve from the AH-6 lamp. The transmission values and areas under the curves gave the relative response characteristics of each filter.

The filters used, their transmission bands, and the transmission values are listed in Table 4-1. The first three values are average transmittances, the last is the ratio of areas under the superimposed curves.

TABLE 4-1

FILTER VALUES FOR ULTRAVIOLET CALIBRATION

Filter No.	Transmission Band, μ	Transmittance
5265	0.25-0.40	0.80
5265	0.70-1.30	0.37
5263	0.70-1.30	0.69
5265	$\frac{0.25\text{-}0.40}{0.25\text{-}0.70}$	0.88 (ratio of areas)

Using the No. 5265 filter as the primary filter, and No. 5263 as a secondary filter, a correction is made for the energy between 0.7 microns and 1.30 microns transmitted by the No. 5265 filter:

$$\text{Correction} = \frac{0.37 \times \text{No. 5263 response}}{0.69}$$

The response of the thermopile to energy between 0.25 μ and 0.40 μ , filtered by No. 5265, is 0.88 of the corrected signal (omitting interreflections):

$$0.88 \left[5265 \text{ response} - \frac{0.37}{0.69} \text{ 5263 response}\right]$$

But this must be corrected for the actual uv transmittance of No. 5265, which is 0.80 energy between 0.25 μ and 0.40 μ incident upon filter (thermopile) =

$$\frac{0.88}{0.80} \left[5265 \text{ response} - 0.54 \text{ (5263 response)}\right]$$

To convert the Eppley thermopile response (mv) to energy (mw/cm^2), it is necessary to divide the Eppley response by the sensitivity of the thermopile, 0.0049 $mv/mw/cm^2$. If equivalent solar units are desired, a second division is necessary. This divisor is 12.42 mw/cm^2/uv sun. Thus, the equation becomes, in units of incident energy in suns:

$$\text{Incident Energy } (0.25\text{-}0.40\mu) = 18.1 \left[5265 \text{ response} - 0.54(5263 \text{ response})\right]$$

$$\text{where } 18.1 = \frac{0.88}{0.80(0.0049)12.42} = K, \text{ the general multiplier constant}$$

The above equation is valid only when the Eppley thermopile is located at the sample position. For measurements outside the simulation chamber two additional corrections were necessary, to determine K^1.

Correction for Sample Distance

Bench measurements of the AH-6 lamp output as a function of distance have shown the intensity follows the inverse square law fairly closely down to 2.5 inches. The correction of distance from detector position to sample position was simply the ratio of Eppley Thermopile responses at the two positions, or 3.15.

Correction for Quartz Window Attenuation

Measurement of the uv lamp energy at the detector position was made with and without the quartz window in the chamber. The ratio of these two responses, when filtered by the No. 5265 filter, was 1.14.

Combination of the two above correction factors 3.15 and 1.14 gives a value of 3.60 for K^1.

Multiplication of the two constants gives a final equation for measurement of the equivalent solar units at the sample position in the Philco Simulation Chamber:

$$\text{suns} = K^1K^2 \ \ 5265 \text{ response} - 0.54(6263 \text{ response})$$
$$= 18.1(3.60) \ \ 5265 \text{ response} - 0.54(5263 \text{ response})$$
$$= 65 \ \ 5265 \text{ response} - 0.54(5263 \text{ response})$$

Using this equation and the two filters, the energy was monitored throughout the prototype test. The results are presented in Figure 4-5. The total exposure in equivalent sun hours (esh) was calculated by breaking the curve into segments and multiplying. The prototype test total exposure was 1880 esh.

4.4 ULTRAVIOLET SOURCE DESIGN EVALUATION

There were no uv lamps burned out during the 765.5 hour test employing the 500 watt lamps. This was much better than previous experience with 1,000 watt lamps. The 500 watt power supply output is ac rather than dc, which could be a major factor in lamp life.

The AH-6 still has the inherent disadvantages of a cooling water requirement, daily monitoring of the output, and a problem of heating samples and surrounding hardware. In addition, the solar spectral match in the uv region is not as good as it should be, because of the lamp deficiency in

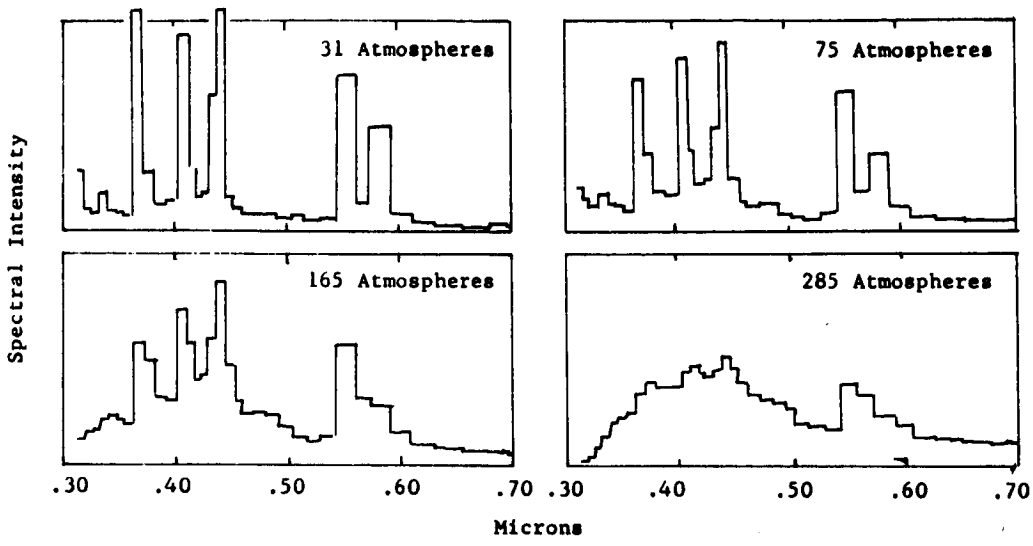

Figure 4-4 Emission Spectra of High Pressure Mercury Arc Lamp at Various Pressure (Ref. 24)

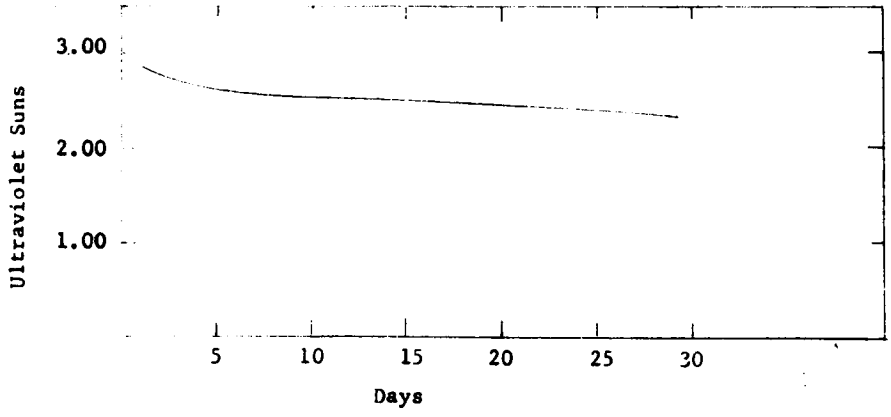

Figure 4-5 Ultraviolet Lamp Degradation (500 Watt AH-6 Type)

some of the wavelengths. The last two problems can be alleviated somewhat in a relative sense by utilizing some combination of copper, nickel, and cobalt filters. This can be accomplished by use of glass filters such as Corning 9863 (Ref. 22) or by addition of various concentrations of chemicals in the lamp cooling water.

SECTION 5

PROTOTYPE TEST

As part of the simulation chamber evaluation, a prototype test was conducted. Because of the interest in and the paucity of data on the effects of low-energy electrons on thermal-control coatings, it was decided to include only this type of material in the prototype test. Actually, the simulator is valuable for testing all types of surface-sensitive materials and components.

5.1 SAMPLE DESCRIPTION

Pre-irradiation measurements were made on six types of samples. Two of these were not included in the final prototype run, at the suggestion of Ames Research Center, in order to obtain greater replication of one sample type. Three types of white coatings were tested, including ZnO-K_2SiO_3, Al_2Si_3-K_2SiO_3, and TiO_2-Al_2O_3-K_2SiO_3 coatings. One specular coating was included, a vapor-deposited aluminum and silicon oxide coating.

A complete tabulation of the samples included in the test may be found in Table 5-1. Sample diameters varied from 7/8" to 1-1/16". Samples were stored in plastic containers and out of direct sunlight at all times except during the irradiation and testing periods, and the samples were handled with tweezers and nylon gloves.

5.2 TEST MATRIX

The test matrix is presented in Table 5-2. The samples were mounted on copper blocks through which heat transfer fluid was pumped. Samples were controlled at two temperatures: (1) ambient temperature ($25^{o}C$ to $38^{o}C$), using water as a coolant, and (2) high temperature,in which the samples were allowed to stabilize in the presence of the ultraviolet lamp heating. This temperature varied from $100^{o}C$ to $160^{o}C$, depending on the thermal properties of the sample.

TABLE 5-1

SAMPLE DESCRIPTION

Sample Type	Composition
A1	$ZnO-K_2SiO_3$, prepared at Ames Research Center. ZnO, 68 parts, (SP-500, New Jersey Zinc Co.) Surface dia: 0.25-0.35 μ - K_2SiO_3, 32 parts (PS-7, Sylvania Co.) Al-6061 substrate. (Six wet-coats of paint sprayed on) Air-Cured at 250°F. Density: 4.7 g/cm^3 Philco No. A1-1 through A1-8 — Ames Batch No. 1-11-9-11
A2	Si_2O_3, 2,000 Å applied over Al, 1 1,000 Å applied over SiO, 1,500 Å applied over Cr, 500 Å applied over Ni substrate 0.030". All vacuum-deposited layers. Identification No.: D101, D106, D109, D110, D113
A3	Al_2SiO_3, 4.4 parts, (Plasma Clay) K_2SiO_3, 1 part, (PS-7, Sylvania Co.) Al substrate, (Wet coats sprayed on) Air-cured at 225°F. Philco No. A3-1 through A3-5 — Ames Identification No. R-101 through H-105
A4	$TiO_2-Al_2O_3-K_2SiO_3$ Philco No. A4-1 — Ames No. MS-117 A4-2 — MS-117 A4-3 — MS-117B A4-4 — MS-117B

TABLE 5-2

TEST MATRIX

	Sample Type			
	ARC-1	DIXX	ARC-3	ARC-4
Irradiated Samples				
High Temp.	1	1	1	1
Low Temp.	2	1	1	1
Electrons Shielded*	1	0	0	0
Control Samples				
Vacuum-treated				
High Temp.	1	1	1	1
Low Temp.	1	1	0	0
Shelf Controls				
Ambiant Temp.	1	1	2	1

* Approximately 66% of the electrons were shielded from this sample. See discussion.

Two A-1 samples ($ZnO-K_2SiO_3$) were shielded with Suprasil quartz, in an attempt to separate the electron and ultraviolet effects. The shield fell off sample A1-4, probably during installation of the flange assembly to the vacuum chamber. The shield over sample A1-3 was composed of five layers of Suprasil, each 0.006" thick and 1" diameter.

5.3 REFLECTANCE MEASUREMENT METHOD

The Perkin Elmer (PE), model 350, double-beam spectrophotometer was used to compare the total reflectances of the samples before and after exposure. The Diffuse Reflectance Accessory, part number 350-0150, was used with a Perkin Elmer-supplied Near Infrared (NIR) adapter to extend the spectral range from 0.750 microns to 2.5 microns.

The PE Reflectance assembly consisted of two identical spheres of approximately 6 inches diameter with 2 inches diameter sample and reference ports. Prior to making any measurements on the PE-350, the spheres were re-smoked (9-23-66) in accordance with specifications provided in the Perkin Elmer Manual No. 990-9221.

Since the samples to be measured were smaller than the 2-inch diameter ports of the spheres, black velveteen masks were fabricated to provide a 3/4-inch diameter port for sample and reference materials 7/8-inch in diameter. Aluminum plates 1/16-inch thick were used with a 3/4-inch diameter hole in the center to accommodate the specimen materials. The inner surfaces of the A1-plates were spot-faced 1/32 inch deep to accept a "smoked" MgO coating so as to minimize any loss of efficiency in the integrating spheres.

Measurements were made in accordance with the procedures and recommendations supplied by the manufacturers of the spectrophotometer in the PE Manual No. 990-9221. Instrument warm-up time was not a factor for consideration because the PE-350 was kept in "stand-by" condition.

5.4 TEST RESULTS

The electron exposure lasted for 765.5 hours, continuously. The exposure conditions for the samples are tabulated in Table 5-3. It is to be noted that samples A1-2, A1-6, D101, D110, A3-4, and A4-3 were, in effect, exposed to the same vacuum and thermal environments as their counterparts at the same chamber station number locations; they were mounted on the back sides of the copper sample holder blocks, facing the chamber walls, however, so were in effect shielded from the electron and ultraviolet sources.

Sample numbers A1-8, D113, A3-3, A3-5, and A4-4 were retained in appropriate storage as shelf samples and are so designated.

Temperature-monitoring thermocouples were installed at every sample station, inserted either in the irradiated sample or in the copper mounting block. The thermocouples used for monitoring the specular samples had to be mounted with the thermocouple junctions in the copper mounting blocks, since the substrates of these four samples were nickel and could not be drilled. Significantly, the highest recorded temperature, 160^{o}C., occurred for the nickel substrate samples A2-3 and A2-4; and the lowest recorded temperature, 25^{o}C., occurred for the nickel substrate samples D101 and D106. These apparent temperature anomolies are attributed to individual difference in heat transfer from samples to blocks and to the thermocouple junction location mandated by these sample forms.

The Suprasil quartz shields over samples A1-3 (0.030"; five layers, 0.006" each) and A1-4 (one layer, 0.006") were not fully effective in stopping the electrons. The sample A1-4 shield fell off at an indeterminate time, as noted previously.

The 0.030" shield of Suprasil over sample A1-3 had a shielding effectiveness of 170 mg/cm^2, which is equivalent to the range of a 0.45 Mev electron (Ref. 2). Essentially, all electrons below 0.45 Mev were stopped by this shield; this constitutes approximately 66 percent of the total number of

TABLE 5-3

SAMPLE EXPOSURE CONDITIONS

Sample No.	Chamber Station No.	Electron Exposure e/cm^2	Ultraviolet Exposure Equiv. Sun Hrs.	Temperature °C Range	Temperature °C Average	Remarks
A1-1	4	1.35×10^{14}	1,880	32-33	32	
A1-2	4	nil	nil	32-33	32	
A1-3 (1)	2	(1.35×10^{14})	(1,880)	25-32	28	Shielded, 0.030 "Suprasil."
A1-4 (2)	3	(1.35×10^{14})	(1,880)	25-32	29	Shielded, 0.006 "Suprasil." Fell off at unknown time.
A1-5	1	1.35×10^{14}	1,880	111-113	112	
A1-6	1	nil	nil	111-113	112	
A1-8	-	-	-	-	-	Shelf sample
D101	5	nil	nil	25-26	26	
D106	5	1.35×10^{14}	1,880	25-26	26	
D109	6	1.35×10^{14}	1,880	146-160	150	TC in sample block
D110	6	nil	nil	146-160	150	TC in sample block
D113	-	-	-	-	-	Shelf sample
A3-1	7	1.35×10^{14}	1,880	32-33	33	TC in sample block
A3-2	8	1.35×10^{14}	1,880	104-118	115	
A3-3	-	-	-	-	-	Shelf sample
A3-4	8	nil	nil	104-118	115	
A3-5	-	-	-	-	-	Shelf sample
A4-1	9	1.35×10^{14}	1,880	37-41	38	
A4-2	10	1.35×10^{14}	1,880	100-108	107	
A4-3	10	nil	nil	100-108	107	
A4-4	-	-	-	-	-	Shelf sample

(1) Electron and ultraviolet dose numbers reduced by the Suprasil quartz shield.

(2) Electron and ultraviolet dose numbers indeterminate due to loss of Suprasil quartz shield at unknown time.

incident electrons. Some decrease in the ultraviolet exposure to sample A1-3 also occurred, due to optical degradation of the Suprasil during the test. Since the optical degradation of the Suprasil was inconsistent with prior industry experience with this material, interpretation of the shielded sample (A1-3; $ZnO-K_2SiO_3$; Z93) degradation was not attempted.

Families of curves representing graphically some of the important results on all four types of samples are presented in Figures 5-1 through 5-4. It is apparent that the aluminum silicate and the titanium oxide-aluminum oxide paints were badly degraded. Changes in reflectance of 20 percent or more occurred in both types of coating, in the important spectral region near 0.45 microns. Since the vacuum-control samples were insignificantly changed, the measured changes in the irradiated samples would have to be due to some type of damage to the coating or to contamination on the coating surfaces.

Degradation is not nearly so apparent in the specular samples and the A-1 samples, although there are indications of slight change in both.

Although it was not the purpose of this contract to evaluate thermal-control materials, the materials which were tested should be exposed again to electrons and ultraviolet to obtain a better evaluation of the degradation. If the contamination proves to be an insignificant factor, the damage could exceed that reasonably predicted from a literature review of previous work with electron and ultraviolet environments (References 1-5 and 23-24).

Infrared emittance was also measured on all samples tested. The emittance was read before and after irradiation on a Lion, Model 25-B, Emissometer. There was no measurable change in the emittance of any of the samples after exposure (Table 5-4) Variations in the data were random and were within the reported accuracy and reproducibility of the Lion Emissometer (Ref. 25)

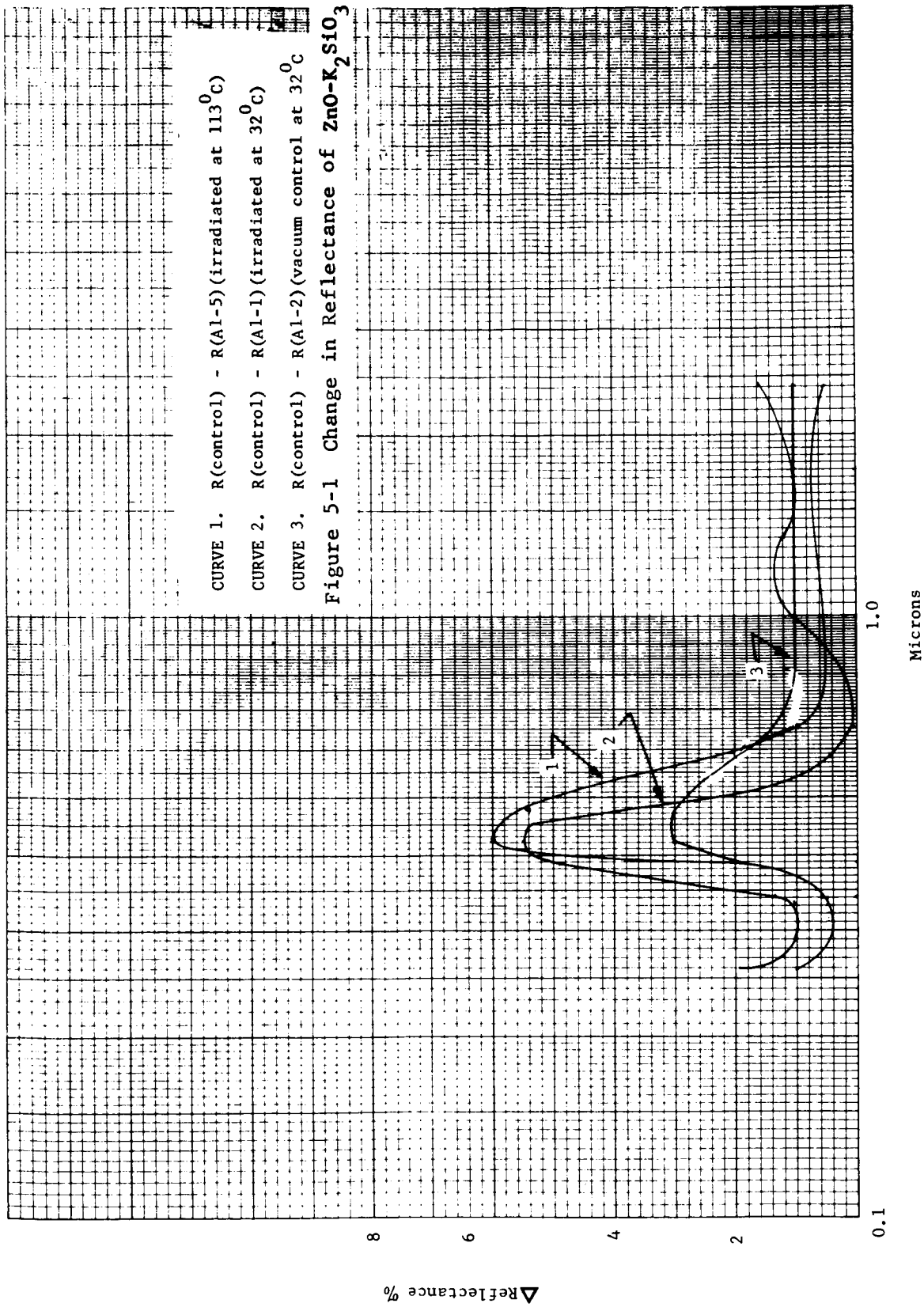

Figure 5-1 Change in Reflectance of $ZnO-K_2SiO_3$

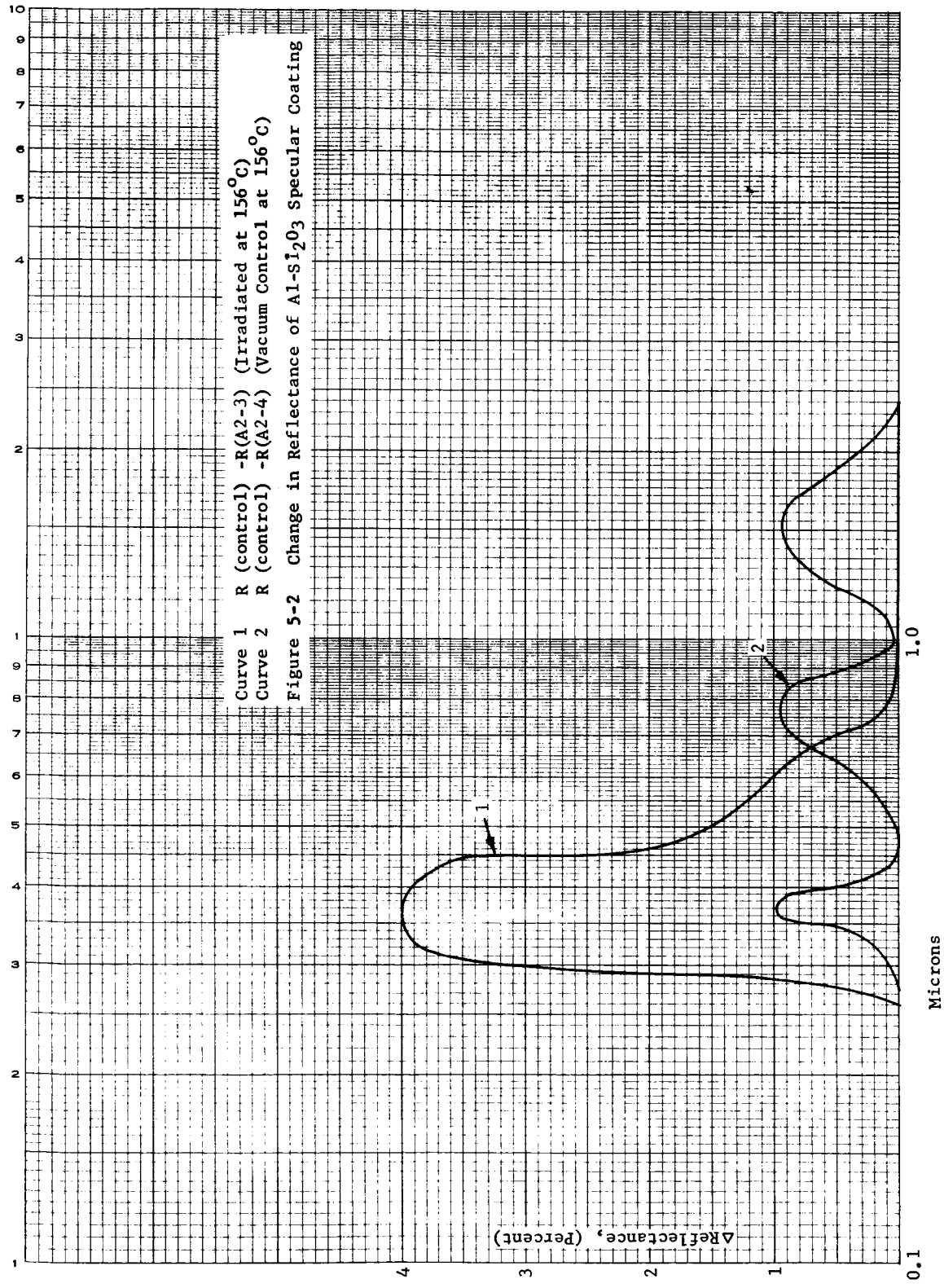
Curve 1 R (control) -R(A2-3) (Irradiated at 156°C)
Curve 2 R (control) -R(A2-4) (Vacuum Control at 156°C)
Figure 5-2 Change in Reflectance of Al-Si2O3 Specular Coating
ΔReflectance, (Percent)
Microns
1.0
0.1
1
2

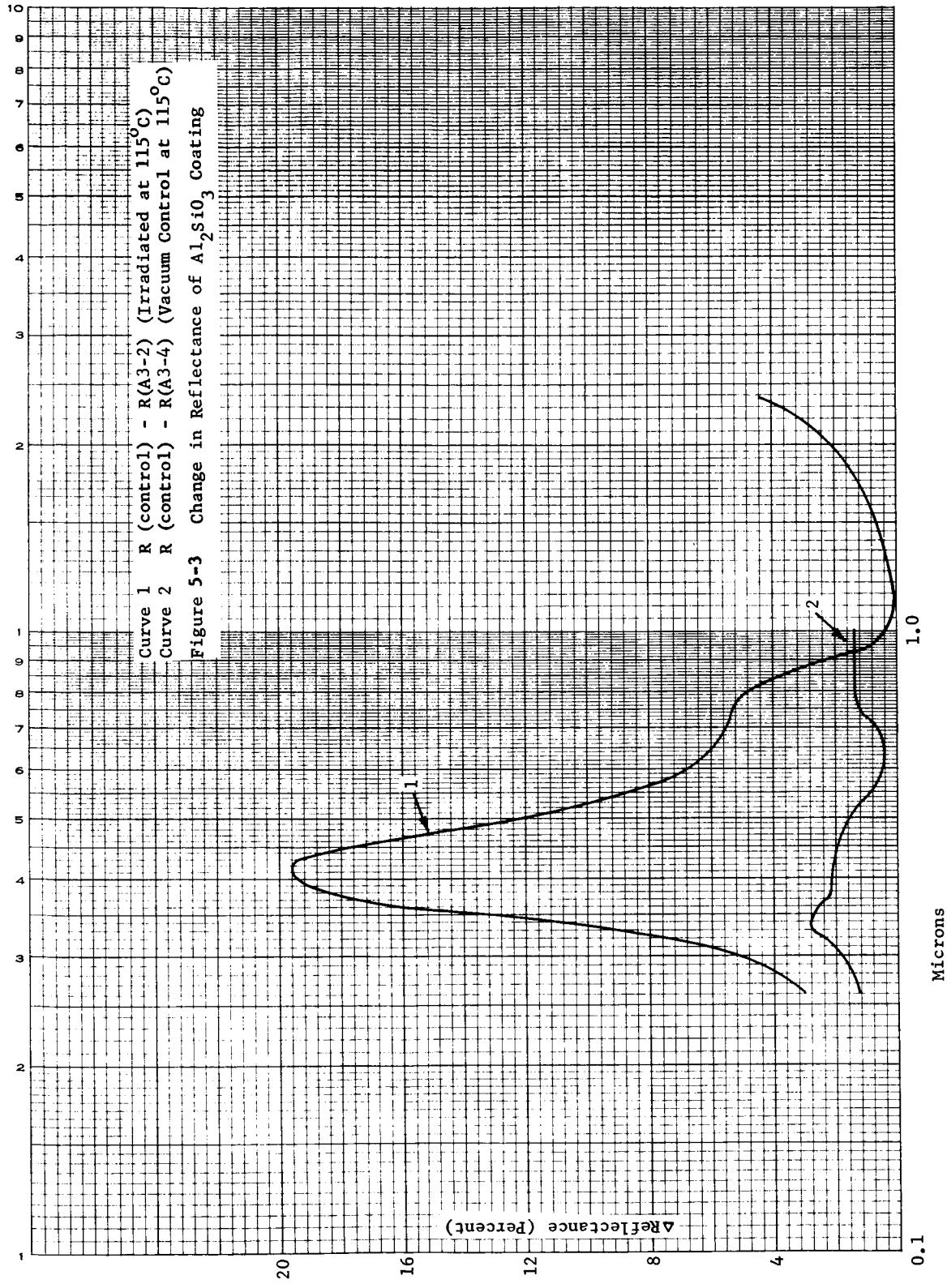

Figure 5-3 Change in Reflectance of Al_2Si0_3 Coating

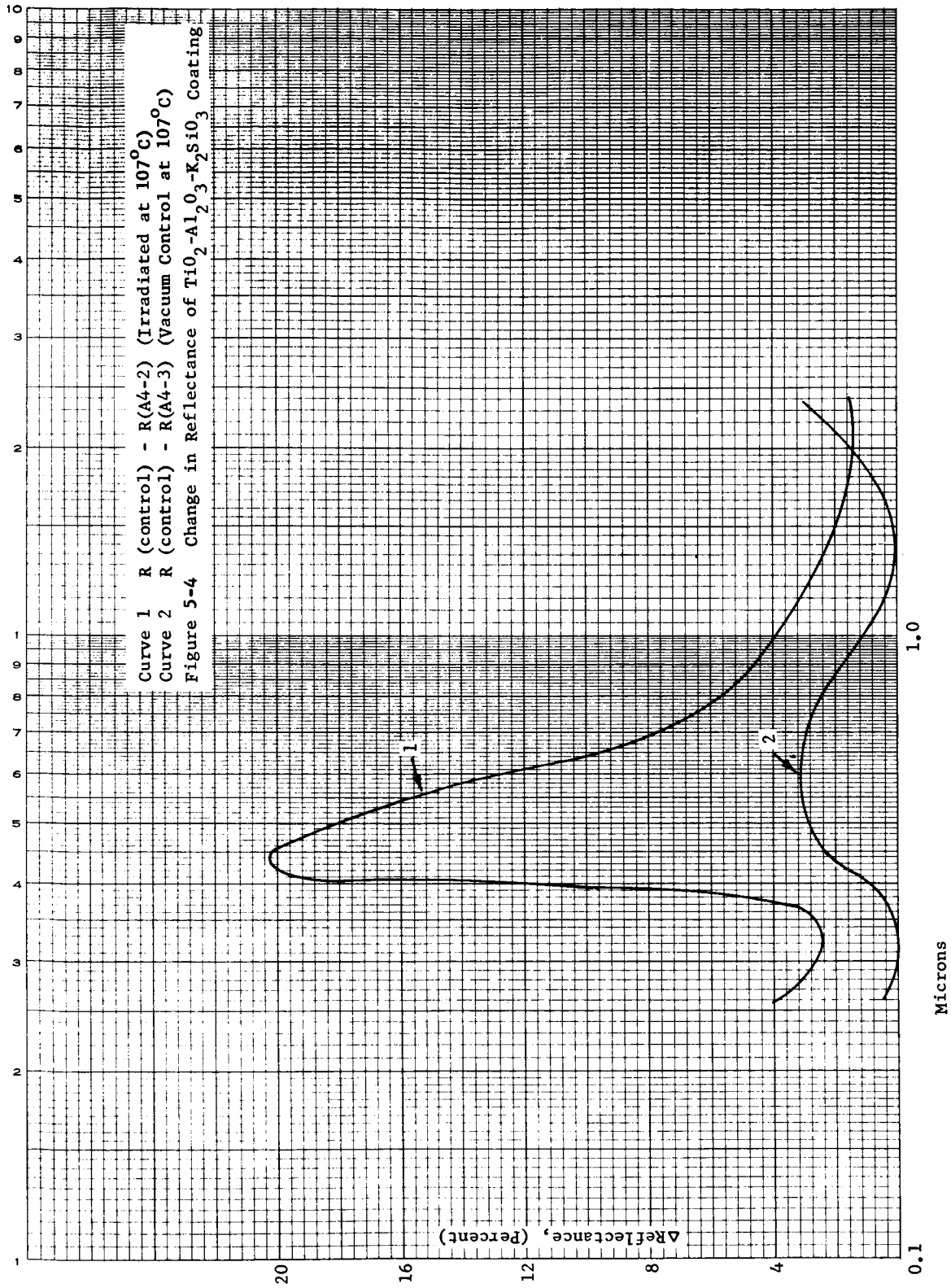
Curve 1 R (control) - R(A4-2) (Irradiated at 107°C)
Curve 2 R (control) - R(A4-3) (Vacuum Control at 107°C)
Figure 5-4 Change in Reflectance of TiO_2-Al_2O_3-K_2SiO_3 Coating
ΔReflectance, (Percent)
Microns
1.0
0.1
1
2

SECTION 6

CONCLUSIONS AND RECOMMENDATIONS

6.1 CONCLUSIONS

The feasibility of using a radioisotope to simulate the space electron environment has been demonstrated. A sealed source of strontium 90 in secular equilibrium with its daughter isotope, yttrium 90, in titanate form, has been incorporated in an existing space environmental simulation chamber, and the resultant electron spectrum has been measured (Figure 3-3); it includes electrons in the 35 Kev to 2.0 Mev range (measured) as indicated. This spectrum compared favorably with the electron spectra for 800, 1,500, and 18,000 nautical mile equatorial orbits (Figures 3-5, 3-6, 3-7).

Flux levels similar to real space environments have been achieved and demonstrated (Figure 3-12). At the sample sites utilized, dosimetry results indicate flux levels on the order of 3×10^7 electrons per square centimeter per second (equivalent 1 Mev electrons). Although the fluxes indicated by dosimetry are below the 1×10^8 e/cm^2-sec with (10 Kev < E < 2.2 Mev) minimum sought, they are deemed adequate to simulate orbital fluxes at this time (Figure 3-9).

Anticipated variations in spatial distribution of the electrons from sample site to sample site due to number of source wires visible (Figure B-1) were not detected. This is attributable to inadequacies in the dosimetry techniques utilized, unknowns in geometrical scattering factors, and/or unrecognized variations of significance in the sample site to source distances.

Solar radiation covering the spectral range from 0.2 to 1.4 microns was provided simultaneously with the electron irradiation at the specimen area. The average source intensity at the sample sites was 2.4 solar constants as provided by a 500 watt AH-6 water cooled mercury vapor lamp.

Representative samples of thermal control materials were irradiated in the combined electron, electromagnetic (uv), vacuum environment for 765.5 hours without interruption.

The degree of vacuum ($< 10^{-6}$ torr) varied for very short periods six times due to failure of the LN_2 trap liquid nitrogen supply system. Since the basic vacuum system is oil diffusion pumped, the potential for sample contamination due to backstreaming of oil molecules from the pump to the chamber was created. Other sources of potential sample contamination included tungsten oxide(s) from the tungsten filament of the nude vacuum gage and tramp radioactive contamination from the isotope source wires. The latter contamination amounted to a maximum of 1,000 decompositions per minute or 35 parts per billion, which is considered insignificant.

6.2 RECOMMENDATIONS

Operation of the prototype chamber for 765.5 continuous hours, coupled with examination of the representative samples at the conclusion of the exposure has led to the following recommendations relative to future work:

a. More precise electron dosimetry methods, directly translatable to total electron dose determination, as well as to energy-deposited dose determinations, should be developed;

b. A "dry" vacuum system should be substituted for the oil-diffusion pumped system;

c. Addition of other beta-emitting isotopes as supplemental sources should be investigated as a means of shaping the simulation flux for matching to specific orbits;

d. Improvement of the existing source wire design in terms of yield (or, source efficiency) and spectral degradation by modification of the cladding(material and thickness) and wire diameter should be investigated;

e. Further development of the present computer technique (COMPOSER) for theoretical prediction of the perturbed spectrum for various radioisotope source material and cladding configurations/combinations to achieve better precision should be accomplished;

f. Comparison of the measured electron spectrum of the existing radioisotope source with additional orbital spectra, non-equatorial, is recommended;

g. Any subsequent chamber designs should incorporate means for in situ measurement of appropriate test sample parameters.

SECTION 7

REFERENCES

1. "Evaluation of Thermal Control Coatings in the Space Environment," AVCO Electronics Division, NASA CR-73028, Dec. 1966.

2. Schmidt, W.F., et al, "Temperature Control Coatings for Cryogenic Temperature Substrates," AFML-TR-66-10, Part 1 (March 1966).

3. Crosby, J.R. and M.A. Perlow, "Snap 10A Thermal Control Coatings," AIAA 65-652, AIAA Conference Monterey (Sept. 1965).

4. Breuch, R.A., et al, "The Effects of Electron Bombardment on the Optical Properties of Spacecraft Temperature Control Coatings," AIAA 65-137, New York (Jan. 1965).

5. Marshall, K.N., et al, "Laboratory and Flight Test Program to Evaluate the Space Stability of Highly Specular Reflective Coatings," AIAA/ASTM/IES Conference, Houston, Texas (Sept. 1966).

6. Hogan, O.H., Zigman, P.E., and Mackin, J.L., "Beta Spectra," USNRDL-TR-802, December 1964.

7. Lamb, Eugene, Oak Ridge National Laboratory Personal Communication.

8. "Radiations from Radioactive Atoms in Frequent Use," U.S. Atomic Energy Commission, 1959.

9. Kaplan, I., Nuclear Physics, First Edition, Addison Wesley Publishing Co., Cambridge, Mass., 1956.

10. Diethorn, W.S., "Sr^{90} -Y^{90} Beta Sources for Radiation Chemistry Studies," International Journal of Applied Radiation and Isotopes, Vol. 12, 1961.

11. Hine and Brownell, Radiation Dosimetry, Chapter 13, Academic Press, 1958.

12. Price, Horton, and Spinney, Radiation Shielding, Pergamon Press, 1957, Pg. 72.

13. Katz, L. and A.S. Penfold, "Range-Energy Relations for Electrons and the Determination of Beta-Ray End-Point Energies by Absorption," Revs. Mod. Phys. 24, 28 (1952).

14. Daniel, H. et al, Physical Review 136 B 1240 (1964)

15. "Investigation of the Use of a Radioisotope for Space Environment Simulation," Philco-Ford WDL Report TR3002, NAS2-3506, Phase I Report.

16. "Investigations of Electron Interactions with Matter," NASA CR-334, December 1965.

17. "Electron Shielding Codes for Evaluation of Space Radiation Hazards," Boeing Report No. D2-90414 (June 1963).

18. "Transmission and Reflection of Electrons by Aluminum Foils," M.J. Berger, NBS Technical Note 187 (April 1963).

19. Tochelin, E., USNRDL (Personal Communication).

20. Charlesby, A. and R.J. Woods, "Radiation Dosimetry with Dyed Cellophane," International Journal of Applied Radiation and Isotopes, 14, 1963 (pp. 414-419).

21. Young, D.E., General Mills (Unpublished Data).

22. Koller, L. R., Ultraviolet Radiation, John Wiley and Sons, New York, (1965).

23. Zerlaut, G.A., et al, "Stable White Coatings," IIT Research Intitute, IIITRI-C6027-16 (1965).

24. Babjak, S.J., C.P. Boebel and A.T. Tweedie, "Combined Space Environmental Effects on Thermal Control Coatings," IEEE Conference on Radiation Effects, Palo Alto, Calif., July, 1966.

25. Gaumer, R.E., et al, "Inspection Tools for Measurement of the Radiation Properties of Satellite Temperature Control Surfaces." Measurements of Thermal Radiation Properties of Solids, NASA SP-31, P. 117 (1963).

APPENDIX A

DEPTH-DOSE SUBROUTINE

APPENDIX A

DEPTH-DOSE SUBROUTINE

Format for Section VI to COMPOSER Program

Subroutine Programming Notes

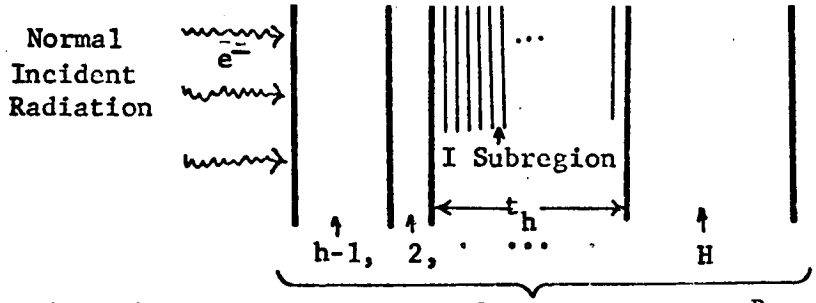

A. Inputs to Subroutine	Range
1. Number of regions of interest = H.	$1 \leq H \leq 99$
Each region, designated by h, has	$1 \leq h \leq H$
thickness t_h cm.	$1.000 \times 10^{-5} \leq t_h \leq 10.0$
2. Each region, h, subdivided into I	$1 \leq I \leq 99$
subregions; numbered small i.	$1 \leq i \leq I$
3. Each region, h, has density, ρ_h,	
uniform over its subregions.	$0.0001 \leq \rho_h \leq 20.0$
4. Subroutine Energy Spectrum Source, S.	$1 \leq S \leq 3$
a. If S = 1, subroutine uses N_j vs $\bar{E}_j$	
from COMPOSER Interpolation	
subroutine output.	
b. If S=2, subroutine uses W_k vs $\bar{E}_k$	
from COMPOSER Electron Shielding	
subroutine output.	
c. If S=3, subroutine uses a special	
deck of new inputs, N_k vs $\bar{E}_k$	$1 \leq k \leq K$
	$1 \leq K \leq 499$

$1.000 \times 10^{1} \leq N \leq 10^{12}$

$0.0001 \leq E \leq 30.00$

B. Calculations

1. Calculate $R_k = (0.2713\ \bar{E}_k^2 + 0.0121)^{\frac{1}{2}} - 0.11$

Note: If S = 1, treat $\bar{E}_j = \bar{E}_k$. If S = 2, recall that R_k is available in Electron Shielding subroutine, although it is probably advisable to recalculate it here.

2. Calculate $R_n = R_{h,i} = \frac{i\ h^t h}{I} \underbrace{+ \sum_{h'=1}^{h-1} h'^t h'}$

where $1 \leq h \leq H$ (add) for $h > 1$

$1 \leq i \leq I$ i.e. (= 0 for h = 1)

$I \leq n \leq HI$

3. $E_{kn} = 0.285\ N_k\ E_k \left[1.85 \left(\frac{R_n}{R_k} - \frac{R_{n-1}}{R_k} \right) + \sin \pi \underbrace{\left(\frac{R_n}{R_k} - 0.31 \right)} - \sin \pi \underbrace{\left(\frac{R_{n-1}}{R_k} - 0.31 \right)} \right]$

Exceptions: a. for n-1 = 0, $R_{n-1} = R_o = 0$

b. for $R_k = 0$, $E_{kn} =$

c. for $\frac{R_n}{R_k} \quad 1$, force $\frac{R_{n-1}}{R_k}$ in the next advancement of n; and all subsequent values of E_{kn} will $\doteq$ 0.)

4. Finally: $E_n = \sum_{k=1}^{k} E_{kn}$

For Units, CALCULATE: $E''_n = 1.60207 \times 10^{-6} E_n \left(\frac{ergs}{cm^2}\right)$

and for each region, h,: $E''_n = \frac{E'_n}{\rho_h} \frac{I}{t_h} \left(\frac{ergs}{gm}\right)$

C. Output: The following printout layout is suggested:

SPECTRUM NO. _____

SHIELD CONFIGURATION NO. _____ (applicable is S=2)

SAMPLE HAS H REGIONS OF INTEREST. H = _____.

EACH REGION IS SUBDIVIDED INTO __I__ SUBREGIONS OF EQUAL THICKNESS.

REGION 1:

THICKNESS = $\underline{t_h = t_1}$ CM.

DENSITY = $\underline{\rho_h = \rho_1}$ G/CM3

SUBREGION	ENERGY ABSORBED IN SUBREGION: ERGS/GM	ERGS/CM2
1	$E''_n = E''_1$	$E'_n = E'_1$
2	E''_2	E'_2
3	E''_3	E'_3
⋮	⋮	⋮
I	E''_I	E'_I
TOTAL: (sum above energies)	_____	_____

REGION 2:

THICKNESS = $\underline{t_h = t_2}$

DENSITY = $\underline{\rho_h = \rho_2}$

SUBREGION	ENERGY ABSORBED IN SUBREGION ERGS/GM	ERGS/CM2
1	$E''_n = E''_{I+1}$	$E'_n = E'_{I+1}$
2	E''_{I+2}	E'_{I+2}
3	E''_{I+3}	E'_{I+3}
⋮	⋮	⋮
	E''_{2I}	E'_{2I}

TOTAL: _____ _____

(sum above energies)

. . .

. . .

. . .

REGION H:

THICKNESS = $\underline{t_h = t_H}$

DENSITY = $\underline{\rho_h = \rho_H}$

SUBREGION	ENERGY ABSORBED IN SUBREGION ERGS/GM	ERGS/CM2
1	$E''_n = E''_{(H-1)I+1}$	$E'_n = E'_{(H-1)I+1}$
2	$E''_{(H-1)I+2}$	$E'_{(H-1)I+2}$
3	$E''_{(H-1)I+3}$	$E'_{(H-1)I+3}$
⋮	⋮	⋮
I	E''_{HI}	E'_{HI}

TOTAL: _____ _____

(sum above energies)

APPENDIX B

THEORETICAL FLUX DISTRIBUTION IN CHAMBER

APPENDIX B

THEORETICAL FLUX DISTRIBUTION IN CHAMBER

This Appendix presents an illustrative calculation of isotope configuration utilized to predict simulator irradiation uniformity at the sample positions. On the basis of these calculations the source wires were slightly separated from the inner cooling cylinder to achieve higher uniformity.

A. STATEMENT OF THE PROBLEM

Four Sr-90 wires are equidistantly spaced on a circle of 1 inch radius. A shielding cylinder of 0.84 inches radius is centered within the circle. At radii of 3, 5 and 7 inches, the discontinuities in the isodose contours due to eclipsing of sources by the cylinder are calculated. The variation in dose at the 5 inch radius location between a point directly opposite the source wires and points 3 inches above and below that point are also calculated.

B. RESULTS OF CALCULATION

Isodose contours at three locations are plotted in Figure B-1. The constant, S, depends on source strength per unit length of the strontium wires. The dose uniformity at various radial distances is as follows:

RADIUS	DOSE VARIATION
3"	$\pm$12.8%
5"	$\pm$14.0%
7"	$\pm$15.5%
Infinity	$\pm$16.7%

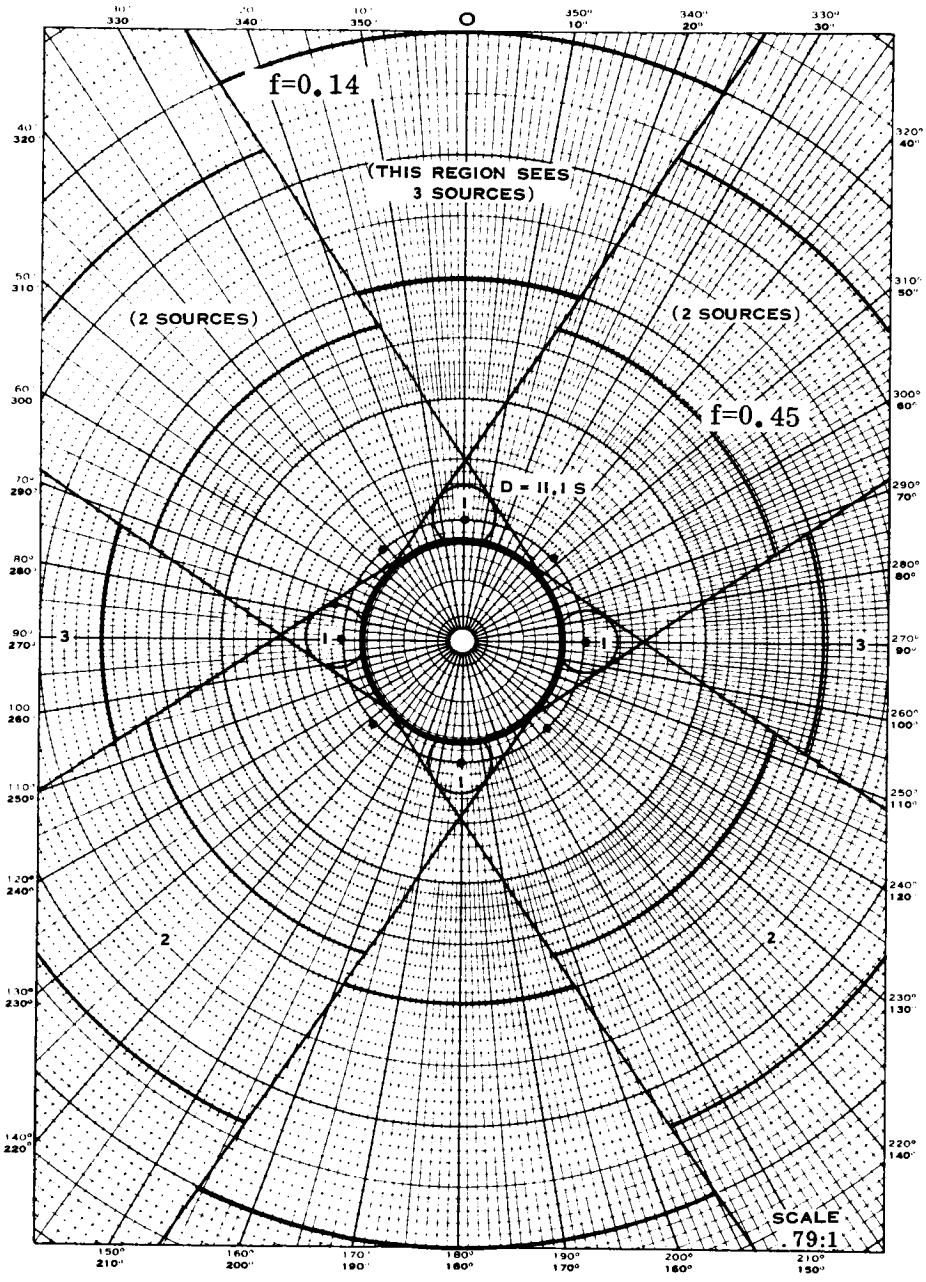

Figure B-1 Isodose Contours - Sources with $1/r^2$ Dependence Mounted on Circle with Larger Diameter than Shielding Cylinder. Maximum Discontinuity (at Infinity) = 33%

The variation in dose at the 5-inch radius as one moves 3 inches away from a circle directly opposite the center of the source wires is 52.6 percent. Stated differently, over the face of a 10-inch diameter concentric cylinder of 6 inch height, the dose is constant to within $\pm$ 26.3 percent.

C. CALCULATION

The radiation dose at (r,θ) is:

$$D = S \sum_i \frac{1}{d_i} \left[\frac{a + L}{\sqrt{(a+L)^2 + d_i^2}} - \frac{a - L}{\sqrt{(a-L)^2 + d_i^2}} \right]$$

where the summation over i includes all source wires visible at the location of (r, θ), and where

$$d_1^2 = r^2 + 1 - 2r \cos \theta$$

$$d_2^2 = r^2 + 1 - 2r \sin \theta$$

$$d_3^2 = r^2 + 1 + 2r \sin \theta$$

The above relations are derived from the cosine law and assume the radius of the source circle equal to unity. The results of the calculation are periodic with period of 45°, so θ need only cover 0° to 45°. There is only one discontinuity per period beyond r = 1.6", and this is best seen by Figure B-2.

a = distance above or below source circle center line to point of interest

2L = length of strontium source wires

d = perpendicular distance from source wire

S = 1/4 x effective source intensity per unit length

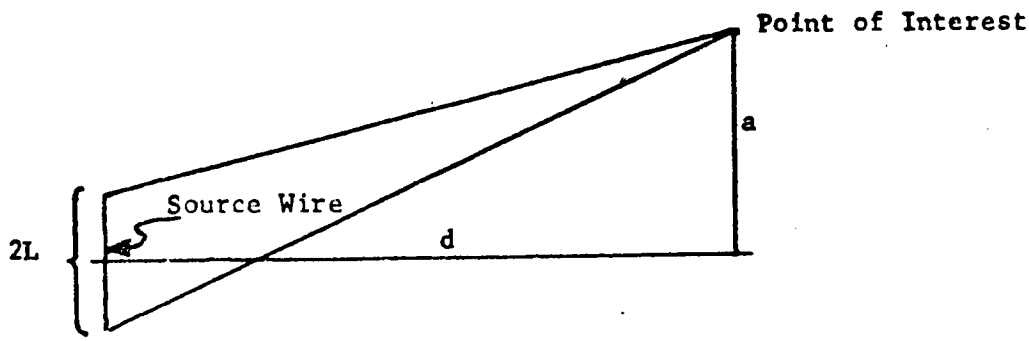

Figure B 2 Geometric Relationships

This could not be confirmed experimentally, due to the limited precision available within the state-of-the-art dosimetry methods. It is also probable that electron scattering off the quartz feed-through and chamber walls smeared the electron flux to a point within the scatter of the experimental dosimetry. In essence, this effect removes any measurable differences in the dose rate among the ten sample positions which are five inches from the centerline.

For a = 0, d_i greater than 3 inches, and L = 0.5 inches (initial design), the term $(L^2 + d_i^2)^{-\frac{1}{2}}$ in the equation for D looks like

$$d_i^{-1} \left(1 - \tfrac{1}{2} \frac{L^2}{d^2}\right) = d_i^{-1} \left(1 - 0.014\right).$$

Thus, beyond a 3-inch radius, the contribution of a 1-inch length of source wire looks like a point source, and we may assume $1/r^2$ attenuation with distance.

The calculation indicates that the dose rate at 5 inches distance of a sample looking at three source rods should be 28 percent higher than one looking at two source rods.

In actuality, when the mapping was complete, it was evident that the electron beam was sufficiently scattered to erase any difference in flux between the sample positions looking at three sources and those looking at two sources. Figure 4-11 shows the actual dose rates at the 5-inch sample position.